Atmospheric
Chemistry
and Physics

The contribution of transport emissions to ozone mixing ratios and methane lifetime in 2015 and 2050 in the Shared Socioeconomic Pathways (SSPs)

Mariano Mertens[1], Sabine Brinkop[1], Phoebe Graf[1], Volker Grewe[1,2], Johannes Hendricks[1], Patrick Jöckel[1], Anna Lanteri[1], Sigrun Matthes[1], Vanessa S. Rieger[1,a], Mattia Righi[1], and Robin N. Thor[1]

[1]Deutsches Zentrum für Luft- und Raumfahrt, Institut für Physik der Atmosphäre, Oberpfaffenhofen, Germany
[2]Faculty of Aerospace Engineering, Section Operations and Environment,
Delft University of Technology, 2629HS, Delft, The Netherlands
[a]now at: University of Vienna, Faculty of Physics, Aerosol Physics
and Environmental Physics, 1090 Vienna, Austria

Correspondence: Mariano Mertens (mariano.mertens@dlr.de)

Abstract. We quantify the contributions of emissions from the transport sector to tropospheric ozone and the hydroxyl radical (OH) by means of model simulations with a global chemistry-climate model equipped with a source attribution method. For the first time we applied a method which also allows for quantifying contributions to OH which is invariant upon disaggregation or recombination and additive. Based on these quantified contributions, we analyse the ozone radiative forcing (RF) and methane lifetime reductions attributable to emissions from the transport sectors. The contributions were analysed for each transport sector separately and for 2015 as well as for 2050 under the Shared Socioeconomic Pathways (SSPs) SSP1-1.9, SSP2-4.5, and SSP3-7.0. In line with previous publications using the source attribution approach, we quantify ozone RF attributable to emissions from land transport, shipping, and aviation for the year 2015 of 121, 60, and 31 mW m^{-2}, respectively. At the same time, we diagnose a relative reduction in methane lifetime due to transport emissions of 14.3 % (land transport), 8.5 % (shipping), and 3.8 % (aviation). These reductions are significantly larger than reported by previous studies due to the application of the source attribution method. Compared to 2015, only SSP1-1.9 shows a strong decrease in ozone RF and methane lifetime reduction attributable to the entire transport sector in 2050. For the projections of SSP2-4.5, we find similar effects of the total transport sector as for 2015, while the effects in SSP3-7.0 increase compared to 2015. This small change in the effects for the two projections compared to 2015 is caused by two main factors. Firstly, aviation emissions are projected to increase in SSP2-4.5 (increase of 107 %) and SSP3-7.0 (+86 %) compared to 2015, resulting in projected ozone RF of 55 mW m^{-2} (+78 %) and 50 mW m^{-2} (+61 %) for the year 2050 from aviation emissions. Secondly, the non-linear effects of atmospheric chemistry in polluted regions such as Europe and North America lead to rather small reductions in ozone and OH in response to emission reductions, especially from land transport emissions. In addition, the increase in emissions from land transport in other parts of the world, particularly in South Asia, leads to an increased contribution of ozone and OH. In particular, ozone formed by land transport emissions from South Asia causes strong RF that partially offsets the reductions in Europe and North America. Moreover, our results show that besides the non-linear response, lack of international cooperation, as in the SSP3-7.0 projection, hinders mitigation of ground-level ozone.

1 Introduction

Emissions from the transport sector, i.e. land transport, shipping, and aviation, affect climate and air quality. The climate is influenced by emissions of both the long-lived greenhouse gas carbon dioxide (CO_2) and short-lived climate forcers such as nitrogen oxides ($NO_x = NO + NO_2$) or particles (Szopa et al., 2021). In contrast to the effects of the CO_2 emissions on the climate, non-CO_2 effects heavily depend on the atmospheric conditions at their emission point and their further transport and chemical transformation in the atmosphere. Examples for such complex processes are the formation of tropospheric ozone or secondary aerosols (Seinfeld and Pandis, 2006) and aerosol–cloud interactions (Bellouin et al., 2020). Tropospheric ozone is a greenhouse gas which also affects air quality and is harmful to humans and vegetation (Monks et al., 2015; Fleming et al., 2018; Mills et al., 2018). Moreover, tropospheric ozone levels are closely linked to the tropospheric oxidation capacity, which determines the lifetime of methane, which also affects climate (e.g. Stevenson et al., 2013).

Tropospheric ozone is formed by photochemical reactions from precursor emissions such as NO_x, carbon monoxide (CO), methane (CH_4), and volatile organic compounds (VOCs). The formation of tropospheric ozone depends on the meteorological conditions and on the ratio of NO_x to VOC concentrations in a non-linear way (e.g. Sillman, 1995; Archibald et al., 2020). Typically, two ozone formation regimes are distinguished: the so-called NO_x-limited regime, in which ozone production increases with increasing NO_x concentrations, and the VOC-limited regime, in which ozone production increases with increasing VOC concentrations but decreases with increasing NO_x concentrations. Due to this non-linear behaviour, a relatively large reduction in precursor emissions will often only result in a relatively small reduction in ozone concentration. Depending on the prevailing chemical regime, emission reductions can even lead to an increase in O_3 in specific regions. Examples of this phenomenon could be observed during the emission reductions as a consequence of the countermeasures against the COVID-19 pandemic: although NO_x emissions were greatly reduced, measurements and results of model simulations showed only a slight decrease in O_3 or, in some cases, regionally increasing O_3 values (e.g. Mertens et al., 2021; Matthias et al., 2021; Grange et al., 2021; Putero et al., 2023).

The emissions of the transport sector are an important source of ozone precursors and other species affecting climate and air quality. Due to various efforts to reduce the effect of the transport sector on climate and air quality, for example shifts towards electric vehicles, the emissions of the transport sector will likely undergo large changes in the future. When designing such mitigation measures for the transport sector, these non-linear processes in atmospheric chemistry need to be considered. In this study, we therefore analyse the contributions of emissions from the three transport sectors – land transport (including road, rail, and inland shipping), aviation, and shipping – to the mixing ratios of ozone and the hydroxyl radical (OH) abundance in the troposphere. We analyse the present-day (2015) conditions and three future projections for 2050 and focus on non-linear changes in ozone and OH caused by emission changes. The year 2050 is chosen because it reflects a time horizon over which large changes in the transport sector are plausible, without exceedingly large speculations into the far future. For the future projections we selected three scenarios among the Shared Socioeconomic Pathways Riahi et al. (SSPs; 2017): a "green" scenario (SSP1; van Vuuren et al., 2017), a middle-of-the-road scenario (SSP2; Fricko et al., 2017), and a scenario of regional rivalry with low mitigative capacities (SSP3; Fujimori et al., 2017). We choose these scenarios as they span a broad range of possible future emission developments. In addition, the differences in the emission totals are large enough to yield different chemical regimes. Hence, we will not focus on the details of the socioeconomic backgrounds and technological pathways behind the chosen scenarios. Rather, we will use the scenarios as a tool to study the chemical effects of transport emissions in different emission scenarios and to derive possible consequences for mitigation strategies. Here, we want to focus on three scientific questions:

- How large are the contributions of transport emissions to tropospheric ozone, and what is their effect on climate?

- How do transport emissions influence the atmospheric oxidation capacity and with this the methane lifetime?

- How do these effects change under different future emission scenarios?

For the analyses, we apply the chemistry-climate model ECHAM/MESSy (European Centre Hamburg general circulation model–Modular Earth Submodel System) Atmospheric Chemistry (EMAC), which is equipped with a tagging technique for source attribution of ozone and ozone precursors including HO_x (Grewe et al., 2017; Rieger et al., 2018). We performed simulations for 2015 and for the three considered SSPs. Each simulation covers 5 years and simulates the same present-day meteorology. Accordingly, the influence of climate change on atmospheric composition is not considered, but the effects on the results are discussed in detail.

This paper adds to the findings of Mertens et al. (2018). In the aforementioned article, a source appointment method, considering NO_x and VOC at the same time, was applied for the first time to quantify the contribution of land transport and shipping emissions to tropospheric ozone. Here, we expand on those findings by adding the following important updates:

- We use a more recent emission inventory including also consistent projections of the emissions for 2050 accord-

ing to CMIP6 (Coupled Model Intercomparison Project Phase 6).

- We integrate the aviation sector to compare the effects of all transport sectors in a consistent way using the same methods.

- We analyse the effects from land transport emissions of different regions.

- We apply a new tagging approach of OH and the hydroperoxyl radical HO_2 (Rieger et al., 2018) to also account for the contributions of transport emissions to OH and their effects on the methane lifetime.

Accordingly, the paper presents, to our knowledge, the first consistent analyses of the effects of transport emissions on tropospheric ozone using a source attribution approach considering all transport sectors and the effects on OH and the methane lifetime.

In this paper, we first describe the model system, the model set-up, and the applied source attribution method in detail and provide a short model evaluation in Sect. 2, followed by a summary of the transport emissions in the SSPs in Sect. 3. Subsequently, we discuss the contribution of the emissions from the three transport sectors to tropospheric ozone (in Sect. 4) and the instances of transport-related ozone radiative forcing (Sect. 5). In Sect. 6, we investigate the contributions of the transport emissions to OH and to the methane lifetime. Finally, limitations of the study are discussed in Sect. 7.

2 Model description, numerical experiments, and evaluation

In the following sections, the EMAC model, the source attribution model, and the numerical experiments will be described in detail. In addition, we will discuss the transport emissions of the three considered SSP narratives.

2.1 The chemistry-climate model EMAC

For the present study, we applied the EMAC chemistry-climate model (Jöckel et al., 2006, 2010, 2016). EMAC uses the second version of the Modular Earth Submodel System (MESSy2) to link multi-institutional computer codes. The core atmospheric model is the fifth-generation European Centre Hamburg general circulation model (ECHAM5; Roeckner et al., 2006). We utilized EMAC (ECHAM5 version 5.3.02, MESSy version d2.54.0.3-pre2.55-02-2077) in the T42L90MA resolution, i.e. with a spherical truncation of T42 (corresponding to a quadratic Gaussian grid of approx. $2.8° \times 2.8°$ in latitude and longitude) with 90 vertical hybrid pressure levels up to 0.01 hPa.

The simulation set-up is very similar to the RC1SD-base-10a simulation described in detail by Jöckel et al. (2016) alongside an evaluation of the resulting model simulations.

Therefore, we describe here only the most important details of the set-up and differences compared to RC1SD-base-10a:

- The applied gas-phase mechanism in the submodel MECCA (Module Efficiently Calculating the Chemistry of the Atmosphere; Sander et al., 2011) incorporates the chemistry of ozone, methane, and odd nitrogen. Alkanes and alkenes are considered up to C_4, while the oxidation of isoprene (C_5H_8) and some non-methane hydrocarbons (NMHCs) are described with the Mainz Isoprene Mechanism, version 1 (von Kuhlmann et al., 2004). The mechanisms of MECCA are part of the Supplement.

- Heterogeneous reactions in the stratosphere (submodel MSBM, Jöckel et al., 2010) as well as aqueous-phase chemistry and scavenging (submodel SCAV, Tost et al., 2006) are included. Photolysis rates are calculated using JVAL (Sander et al., 2014).

- Emissions of methane (CH_4), the long-lived greenhouse gases (CO_2, N_2O, etc.), and the ozone-depleting substances (ODSs) are not considered explicitly. Instead, pseudo-emissions of these emissions are calculated using the submodel TNUDGE (Kerkweg et al., 2006). TNUDGE relaxes mixing ratios in the lowest model layer towards prescribed mixing ratios using Newtonian relaxation (see also Jöckel et al., 2016).

- Dry deposition is considered via the submodel DDEP (described as DRYDEP by Kerkweg et al., 2006). It is based on the big-leaf approach by Wesely and Hicks (2000).

- The emissions of lightning NO_x depend on the meteorology and are parameterized after Grewe et al. (2001), resulting in global total emissions of $\approx 4.5\,Tg\,(N)\,a^{-1}$. This value is well in the range of the best estimate given by Schumann and Huntrieser (2007) that is based on a review of observational and modelling approaches.

- Emissions of NO_x from soil and biogenic C_5H_8 emissions also depend on the meteorology and are calculated using the MESSy submodel ONEMIS (Kerkweg et al., 2006), following the parameterizations by Yienger and Levy (1995) for soil NO_x and Guenther et al. (1995) for biogenic C_5H_8.

- The radiation is largely based on the original radiation scheme from ECHAM5 (Roeckner et al., 2003) but has been restructured and expanded with additional features such as multiple diagnostic calls as described by Dietmüller et al. (2016).

- The land surface model and the boundary layer implementation are modularized versions (see also Jöckel et al., 2016) of the original implementations of ECHAM5 described in detail by Roeckner et al. (2003).

2.2 Source attribution method

The TAGGING method has been applied in numerous studies to quantify the effects of the transport sectors on tropospheric ozone (Mertens et al., 2018, 2020a, b; Matthes et al., 2021; Mertens et al., 2021; Maruhashi et al., 2024). The concept of the source attribution methods (also known as tagging or labelling methods) fundamentally differs from the concept of perturbation methods (also known as zero out, brute force, etc.; Wang et al., 2009; Grewe et al., 2010; Clappier et al., 2017; Mertens et al., 2020b).

In this study, ozone and its precursors are attributed to 18 source categories which are listed in Table 1. Most of these categories refer to specific emission sectors, but some others (for example the production of ozone in the stratosphere) do not refer to such sectors. For land transport and anthropogenic non-traffic emissions we differentiate between five different geographical source regions (see Sect. S8 in the Supplement for detailed definition). These are

- Europe (EU)

- North America (NA)

- South Asia (SA)

- East Asia (EA)

- rest of the world (ROW).

For better readability, we denote absolute contributions as superscripted abbreviations. For example, O_3^{SHP} and OH^{SHP} denote the absolute contributions of shipping emissions to O_3 and OH mixing ratios, respectively. In addition to the abbreviations given in Table 1, we define the abbreviation "TRA", indicating the contribution of land transport emissions from all regions (i.e. the sum of land transport from Europe, North America, East Asia, South Asia, and the rest of the world). Relative contributions are defined as the mixing ratios of a specific category (e.g. O_3^{SHP}) divided by the total mixing ratio of the species (e.g. O_3). Since the budget of the tagged species is closed, the relative contribution of the sum over all categories for each considered species yields 100 %. For example, the relative contribution of shipping emissions to ozone, denoted as $C^{SHP}(O_3)$, in percent, is defined as

$$C^{SHP}(O_3) = 100 \cdot \frac{O_3^{SHP}}{O_3}. \tag{1}$$

2.3 Radiative forcing calculations

Based on the diagnosed ozone contributions, we calculate the contribution of each category to the radiative flux (stratospherically adjusted) at the top of the atmosphere during model runtime using multiple diagnostic calls of the radiation routines (submodel RAD, Dietmüller et al., 2016). In the

following, we refer to this contribution to the radiative flux as the "radiative forcing (denoted as RF) of the respective emission category". As discussed in detail by Mertens et al. (2018) our definition of the RF does not take into account the change in ozone since pre-industrial times (see Forster et al., 2021), as we do not perform a pre-industrial simulation. Instead, the ozone RF in each simulation is decomposed into the respective contributions from the 18 source categories for present-day and future conditions (see also Dahlmann et al., 2011). The change in ozone attributed to natural sources between pre-industrial and present-day levels caused by the increase in anthropogenic emissions and the respective effects on the ozone chemistry is not considered (see a detailed discussion in the Supplement of Mertens et al., 2018).

A detailed description of the procedure to calculate the RF is given by Mertens et al. (2018). Here we recall only the most important aspects, exemplarily for the shipping (SHP) sector.

1. $\Delta O_3^{SHP} = O_3 - O_3^{SHP}$ is calculated.

2. Stratospherically adjusted radiative fluxes are calculated at every radiation time step (i.e. every third model time step) for O_3 and ΔO_3^{SHP}.

3. In post-processing, the radiative contribution is calculated by subtracting the radiative flux (rflux) at the top of the atmosphere:

$$RF_{O3}^{SHP} = \texttt{rflux}(O_3) - \texttt{rflux}(\Delta O_3^{SHP}). \tag{2}$$

It is important to note that neither the radiative fluxes from O_3 nor the ozone contributions (e.g. O_3^{SHP}) feed back onto the dynamics. Instead, prescribed climatologies are used for the forcing of the dynamics (as described in Sect. 2.4).

2.4 Numerical experiments and emissions

For the present study, four different numerical experiments were performed as summarized in Table 2. Each simulation has been conducted for the period July 2012–December 2017. The year 2012 is considered spin-up, and the years 2013–2017 are analysed. The chemical tracers, the tagging tracers, and water vapour are initialized in all simulations from a 1.5-year-long spin-up simulation. This initialization is the same in each simulation.

EMAC is nudged by Newtonian relaxation of temperature, divergence, and vorticity and the logarithm of surface pressure (Jöckel et al., 2006) towards ERA-Interim reanalysis data (Dee et al., 2011). Furthermore, the sea surface temperature and sea ice coverage are prescribed as transient time series from ERA-Interim.

To allow for identical, even binary-identical, meteorological conditions in all simulations, the quasi chemistry-transport model mode (QCTM mode; Deckert et al., 2011) of EMAC is used. The use of QCTM mode enables us to

Table 1. Overview of the categories for the tagging source attribution applied in this study. Detailed definitions of the categories are given by Grewe et al. (2017). IPCC: Intergovernmental Panel on Climate Change.

Name	Abbreviation	Description
Anthropogenic non-traffic Europe	IN*-EU	Anthropogenic emissions not related to transport from Europe
Anthropogenic non-traffic North America	IN-NA	Anthropogenic emissions not related to transport from North America
Anthropogenic non-traffic South Asia	IN-SA	Anthropogenic emissions not related to transport from South Asia
Anthropogenic non-traffic East Asia	IN-EA	Anthropogenic emissions not related to transport from East Asia
Anthropogenic non-traffic ROW	IN-ROW	Anthropogenic emissions not related to transport from the rest of the world (ROW)
Land transport Europe	LT-EU	Land transport emissions from Europe
Land transport North America	LT-NA	Land transport emissions from North America
Land transport South Asia	LT-SA	Land transport emissions from South Asia
Land transport East Asia	LT-EA	Land transport emissions from East Asia
Land transport ROW	LT-ROW	Land transport (IPCC codes 1A3b_c_e) emissions from the rest of the world
Land transport total	TRA	The category is not tagged individually but calculated as the sum of LT-EU, LT-NA, LT-SA, LT-EA, and LT-ROW
Shipping	SHP	Global shipping emissions (IPCC code 1A3d)
Aviation	AIR	Global aviation emissions
Stratosphere	STR	Downward transport from the stratosphere (more specifically, production of ozone by O_2)
Biogenic	SOIL	Biogenic emissions and soil NO_x
Biomass burning	BB	Emissions from biomass burning
CH_4	CH_4	Degradation of CH_4 as a source of NMHCs
N_2O	N_2O	Degradation of N_2O as a source of NO_y
Lightning	LIG	Emissions of lightning NO_x

* The abbreviation IN stands for industry, but the category anthropogenic non-traffic contains all non-traffic-related activities, i.e. industry, households, energy, and agriculture including agricultural waste burning.

Table 2. Overview of the performed numerical simulations. PD: present day.

Name	Emission scenario	Emission year	Meteorology
PD	SSP2-4.5	2015	Jul 2012–Dec 2017
SSP1-1.9	SSP2-4.5	2050	Jul 2012–Dec 2017
SSP2-4.5	SSP1-1.9	2050	Jul 2012–Dec 2017
SSP3-7.0	SSP3-7.0	2050	Jul 2012–Dec 2017

quantify signals also for very small emission perturbations, which otherwise (i.e. with a full coupling of chemistry and dynamics) would be hard to detect in a statistically significant way or would need very long integration times. In this mode, mixing ratios of the radiatively active trace gases are prescribed for the radiation calculations. This means that in each simulation the same instances of radiative forcing by the prescribed mixing ratios are considered. Furthermore, mixing ratios of the chemical species are prescribed for the processes responsible for the coupling of the chemistry with the hydrological cycle. The prescribed mixing ratios are monthly averages taken from a previous model simulation performed with the PD set-up but with full coupling of chemistry and dynamics.

The simulations are performed as time slices, meaning that prescribed monthly emissions for 2015 or 2050 are repeated every year. For each simulation, the emissions of short-lived chemical species (NO_x, NH_3, SO_2, CO, and VOC) from biomass burning, anthropogenic non-traffic sources, land transport, shipping, and aviation sectors are taken from the respective emission scenarios. The emissions of longer-lived species (including methane) and ozone-depleting substances, which are nudged as described in Sect. 2.1, are taken from the SSP2-4.5 emission inventory for 2015. Emissions of soil NO_x, biogenic isoprene, and lightning NO_x are calculated online, driven by the meteorological conditions, and are therefore identical in each simulation. The transport emissions in the simulations are discussed in detail in Sect. 3, including an analysis of the NO_x emission totals. More information on the applied emissions (also for CO and VOC) is given in Sect. S1 in the Supplement.

2.5 Model evaluation

The EMAC model has been extensively evaluated in the past. Jöckel et al. (2016) present a detailed evaluation of various atmospheric variables, including tropospheric and stratospheric ozone. From these evaluations we know that EMAC has a positive bias for tropospheric ozone and a negative bias for carbon monoxide. Estimates of the methane lifetime simulated by EMAC are typically at the lower end of the range of values estimated by other models. However, multi-model inter-comparisons show that the biases compared to observa-

tional data of EMAC are within the range of those of comparable models (Naik et al., 2013; Stevenson et al., 2013; Voulgarakis et al., 2013; Young et al., 2013).

Given these extensive previous evaluation efforts, we reduce the evaluation of our model results to a minimum. In a first step we compare the ozone mixing ratios of the results from our PD simulation with the results of the RC1SD-base-10a simulation discussed by Jöckel et al. (2016). The set-up of both simulations is very similar, despite changes in the emission inventories, small updates and bug fixes in the model infrastructure, and the fact that we simulate more recent years. Ozone is larger by 2–4 nmol mol^{-1} in PD compared to RC1SD-base-10a in the extra-tropical lower and middle troposphere. In the extra-tropical free troposphere the difference between the two simulations is slightly larger, reaching up to 8 nmol mol^{-1}. In the tropical troposphere the difference ranges between -2–2 nmol mol^{-1}. Overall, the change is lower than 8 % with the largest increase in the Southern Hemisphere dominated by the variability in the polar vortex. Figures of the comparison of ozone and of further trace gases are provided in the Supplement (see Sect. S10 in the Supplement). From this analysis we conclude that the extensive evaluation presented by Jöckel et al. (2016) remains valid.

In addition, we compared the simulated ozone mixing ratios in the upper troposphere and lower stratosphere (UTLS) with satellite measurements published as the Stratospheric Water and Ozone Satellite Homogenized (SWOOSH) dataset by Davis et al. (2016). The SWOOSH data are a homogenized, gridded, monthly-mean dataset for ozone and water vapour based on various satellite data. For the considered period the dataset is based on the Aura Microwave Limb Sounder (MLS). We used the SWOOSH data in version 2.6 with a horizontal resolution of 2.5° and 31 vertical levels. Horizontally, the SWOOSH data are interpolated onto the slightly coarser EMAC grid; vertically, the data are interpolated onto the much coarser SWOOSH grid in a fashion similar to Pletzer and Grewe (2024). The monthly-mean SWOOSH data are compared with monthly-mean data from the model, meaning that satellite data and model data are not co-located in space and time. Averaging kernels of the satellite are not considered; accordingly, the satellite data can only be used for qualitative evaluation. The evaluation is performed for the years 2013–2017.

Figure A1 shows the difference between the ozone mixing ratios of the PD simulation and the SWOOSH data. Overall, the inter-comparison confirms the known bias of simulated ozone, as discussed above, also in the upper troposphere. We would like to stress that the results can only be used for qualitative evaluation (i.e. confirming the ozone bias), as averaging kernels are not used, nor are the data spatially and temporally co-located. Moreover, the number of considered years are very limited, and we found that the magnitude and location of the peak of the upper-tropospheric ozone bias strongly depend on the approach used for vertical remapping due to

the limited vertical resolution of SWOOSH. For a detailed quantitative evaluation of UTLS ozone we refer to previous inter-comparisons, for example the IAGOS (In-service Aircraft for a Global Observing System; in situ measurements on board passenger aircraft) measurements presented by Jöckel et al. (2016), Pletzer et al. (2022), and Cohen et al. (2024).

3 Transport emissions in the SSP projections

In our study, we consider three specific emission scenarios among the various combinations of SSP projections and forcing pathways (Gidden et al., 2019):

– SSP1-1.9 – a version of the SSP1 narrative with a target radiative forcing from anthropogenic emissions of 1.9 W m^{-2} in 2100

– SSP2-4.5 – a version of the SSP2 narrative with a target radiative forcing from anthropogenic emissions of 4.5 W m^{-2} in 2100

– SSP3-7.0 – a version of the SSP3 narrative with a target radiative forcing from anthropogenic emissions of 7.0 W m^{-2} in 2100.

The narratives of these SSPs can be summarized as follows (O'Neill et al., 2017).

– *SSP1 (sustainability)*. SSP1 features relatively low population growth with medium–high economic growth per capita. There is moderate international trade and effective international cooperation, and policy focuses on sustainable development. Technological development is rapid, with a strong shift away from fossil fuels and towards efficiency and renewable energy.

– *SSP2 (middle of the road)*. SSP2 features medium population growth and medium economic growth per capita. International cooperation is relatively weak, and international trade is moderate. Environmental policy focuses on local pollutants, but there is only a weak focus on sustainability. Accordingly, there is only some investment in renewable energy, and fossil fuels continue to play an important role. Technological development is medium and distributed unevenly, with a slow transfer of technologies.

– *SSP3 (regional rivalry)*. SSP3 features high fertility in the groups of low- and high-fertility countries and low fertility in the group of rich OECD (Organisation for Economic Co-operation and Development) countries (see Table 1 in KC and Lutz, 2017). Economic growth per capita is slow, and there is high inequality across countries. De-globalization takes place, and international trade is strongly constrained. International cooperation is weak, and environmental issues are considered low priority. Technological development is slow,

with little technological change directed towards domestic energy sources.

The traffic emissions of air pollutants between the three projections differ strongly, as they depend on mobility, global trade, and applied technologies. Overall, in 2050, passenger travel demand is largest in SSP2, followed by SSP1 and SSP3. Cars are an important transportation mode in all three SSPs, with the largest passenger travel demand in SSP2, followed by SSP3 and SSP1. In SSP1, public transport (bus and train) plays a more important role than in SSP2 and SSP3. Moreover, SSP1 features the lowest demand for aviation, followed by SSP3 and SSP2. High-speed trains become more important as an alternative mode of transportation in SSP1 (see Fig. 5 in van Vuuren et al., 2017). SSP1 has the overall lowest energy demand for the transport sector, followed by SSP2 and SSP3. Even though the energy demand of the transport sector in SSP1 is lower than in SSP3, SSP1 has the larger transport demand. This shows that a decoupling of energy demand and passenger demand is achievable in a sustainable scenario. In all SSPs, liquid fuels dominate the overall energy demand for transportation in all scenarios until ~ 2040. Only in SSP1 does the electrification of cars increase compared to the present day before 2040. In this scenario, hydrogen also becomes an important energy carrier in the transport sector after 2050. In the SSP3 projection, even in 2050, only very little electrification is projected in the transport sector, while the SSP2 projection assumes a moderate amount of electrification (see Fig. S13 in the Supplement of Bauer et al., 2017). Generally, SSP1 features a maximum electrification of 75 % of total transport, while SSP2 and SSP3 feature 50 % and 10 % maximum electrification, respectively (Fricko et al., 2017).

In addition to the adaptation of alternative energy sources, such as electricity, in the transport sector, air pollutant emissions depend heavily on the regulations that are enacted. Different pollution control levels have been defined which are linked with the SSP narratives (Rao et al., 2017).

- *SSP1*. Policy-makers aim for much lower air pollution levels over the 21st century than current legislation targets. There is a strong concern for negative effects of air pollutants on health and ecosystems. Moreover, medium- and low-income countries catch up relatively quickly with industrialized countries in terms of pollution control.

- *SSP2*. The general trend of emission reductions is continued worldwide, and the pollution concentration targets become more ambitious with increasing income over the century. There is increasing concern for the effects of pollutants on human health and the ecosystems. Due to the diffusion of technology and knowledge, developing countries reach levels of emission control relatively early compared to historical developments in OECD countries. Regions with large population densities may not reach the targeted air pollution levels.

- *SSP3*. Compared to SSP2, the implementation of pollution control is delayed. Moreover, due to less international cooperation and the slow deployment of international laws, technologies are developed less quickly and trans-boundary pollution (e.g. hemispheric transport of air pollutants) increases.

The integrated assessment models (IAMs) behind the SSPs do not apply complex air pollution control technologies. Therefore, the pollution control scenarios are implemented in a simplified approach based on trajectories of the emission factors (Rao et al., 2017). The trajectories are based on two sets of emission factors. The first set is "current legislation" (CLE), assuming efficient implementation of existing environmental legislation. The second set is the maximum technically feasible reduction (MFTR) set. The near-term achievement of MFTR is not considered feasible, but it serves as a baseline for what is ultimately possible given the current state of air pollution control technologies.

SSP2 assumes the implementation of CLE until 2030, while SSP1 (SSP3) assumes a stronger (less strict) implementation of CLE until 2030, respectively. After 2030, the progress of the emission factors depends on the level of technological progress, i.e. the progress towards MFTR emission factors. In addition, depending on their economic developments, non-OECD countries can catch up with OECD countries with respect to the implementation of air pollution control faster (SSP1) or slower (SSP3). In all scenarios, the MFTR emission factors are stagnant in time, which means that there is no speculation about possible future technologies better than MFTR. Thus, in countries and SSPs with a high penetration of MFTR, this might be a conservative scenario (Rao et al., 2017).

In all SSP projections, the spatial distribution of the land transport emissions is taken from the EDGAR (Emissions Database for Global Atmospheric Research; Janssens-Maenhout et al., 2019) 4.3.2 emission inventory, aviation emissions are distributed as in CMIP5 (Coupled Model Intercomparison Project Phase 5; Taylor et al., 2012), and shipping emissions are distributed according to ECLIPSE (Evaluating the Climate and Air Quality Impacts of Short-Lived Pollutants; Stohl et al., 2015). The spatial distribution of land transport and aviation emissions is constant in time. Shipping emissions use projected changes in sulfur emissions due to changes in sulfur content and the definition of the sulfur emission control area (SECA). More details on the regridding process of the CMIP6 emissions are given by Feng et al. (2020). We apply the aviation emissions in their original form which have an error in the geographical distribution, as recently reported by Thor et al. (2023). The corrected emissions would lead to an increase in the ozone RF of 7.6 %.

Figure 1 displays the NO_x emissions in the four simulations. Tables of the total emissions for NO_x, VOC, and CO

emissions are part of the Supplement (Sect. S1). Further analyses of the changes in the total emissions in the SSP projections are given by Righi et al. (2023).

In the SSP1-1.9 projection for 2050, anthropogenic NO_x emissions reduce by more than 70 % compared to 2015, which is in agreement with the underlying narrative. In particular, the emissions in the transport sector decrease strongly by around 90 % for most land transport regions, around 95 % for the shipping sector, and 64 % for the aviation sector. The reductions are caused by transformations of the transport system and by alternative fuels (e.g. electrification). Generally, SSP1 features a much larger share of public transport (e.g. buses and trains) in 2050 compared to the other SSPs (van Vuuren et al., 2017), and the aviation sector has a lower passenger demand compared to SSP2 and SSP3. In addition to this high share of public transport and the quick shift towards alternative technologies, SSP1 also features the strongest air pollution control among the considered scenarios.

In the SSP2-4.5 projection for 2050, anthropogenic NO_x emissions decrease by around 25 %, but emission peaks are shifted regionally compared to 2015. As an example, land transport emissions decrease in most regions but strongly increase over South Asia (around 60 %) and over Africa. The decrease is mainly caused by stronger air pollution control, especially in the OECD regions, while the increase is partly caused by increases in the population in South Asia and parts of Africa. The aviation emissions are doubled compared to 2015, which is consistent with the increase in passenger travel demand in the aviation sector. Shipping emissions are reduced by around 30 %. These reductions mainly take place around Europe and the eastern coast of North America, while emissions increase, especially along the main shipping routes from China to Singapore. Most of the reductions are likely due to technological improvements (including increased air pollution control).

The SSP3-7.0 projection for 2050 exhibits around 12 % higher anthropogenic NO_x emissions compared to 2015. The regional changes, however, differ strongly. For example, the land transport NO_x emissions decrease in Europe and North America compared to 2015 by around 40 % and 50 %, respectively, as a consequence of the stronger air pollution control (including technological advancements) in these regions. In South Asia, the NO_x emissions from land transport increase by almost 100 %, and in the rest of the world they increase by around 40 %. One reason for the particularly strong increase in South Asia is the strong population growth, in particular in India, in SSP2 and SSP3 in 2050 compared to 2015 (KC and Lutz, 2017). In addition, air pollution control is limited in SSP3. The shipping emissions for 2050 are lower in SSP3 compared to SSP2, even though air pollution control is less strict in SSP3 compared to SSP2. This is likely caused by the strong decrease in international trade between the regions in SSP3 (Fujimori et al., 2017; Bauer et al., 2017).
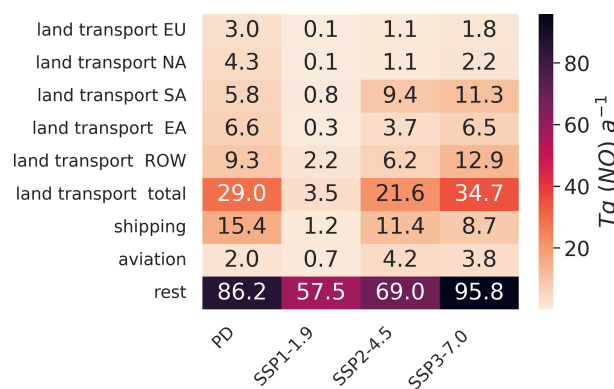

Figure 1. Comparison of the NO_x emissions (in Tg (NO) a^{-1}) between the four performed simulations for 2015 (PD) and 2050 (projections; see Sect. 2.4 for a detailed description). The land transport emissions are given for the different source regions and as global totals ("land transport total"). The category "rest" indicates all other emission sources, also including soil and lightning NO_x emissions which are not included in the SSP emission data. Please note that the land transport total emissions are only given for comparison; they are not emitted in addition to the regional land transport emissions.

4 Contributions to ground-level ozone

We first analyse the general changes in ground-level ozone for the three projections compared to 2015 (Sect. 4.1), which is followed by an analysis of the individual transportation sectors in detail in Sects. 4.2 to 4.4. In these analyses the contributions to ground-level ozone (land transport and shipping) and zonally averaged contributions to ozone (aviation) are analysed. Moreover, we quantify the trends of the absolute contributions from land transport and shipping emissions to ground-level ozone for specific geographical regions. For the aviation sector we focus on the zonal means of the relative contributions and the trends of the contribution of aviation ozone to the tropospheric ozone column for main flight regions. Moreover, we quantify the changes in the ozone burden caused by the changes in the emissions in Sect. 4.5.

4.1 Changes in ground-level ozone

Figure 2 shows the ground-level ozone mixing ratios for 2015 and the changes in the ground-level ozone mixing ratios compared to 2015 for the three projections in 2050. Figures of the ground-level ozone mixing ratios for the projections are part of the Supplement (Sect. S2).

In 2050, ozone decreases in the SSP2-4.5 projection compared to 2015 in most regions by 2–6 nmol mol^{-1}. However, ozone increases slightly over Central Africa, around India, along the eastern coast of China, and in central Europe. Especially in central Europe and China is the increase due to decreased ozone titration caused by decreasing NO_x emissions. For the SSP3-7.0 projection, ozone increases strongly in 2050 compared to 2015. The increase reaches

up to 10 nmol mol^{-1} and particularly affects West Africa, the Arabian Peninsula, India, and Southeast Asia. In contrast to this, ground-level ozone decreases strongly in 2050 for the SSP1-1.9 projection compared to 2015. In most regions the decrease is in the range of 10–15 nmol mol^{-1}, and it exceeds 20 nmol mol^{-1} on the Arabian Peninsula. The general changes in ground-level ozone for the three projections and regional features, such as the strong increase in ozone over Asia in SSP3-7.0, are in agreement with the analyses of CMIP6 simulation results by Turnock et al. (2020). However, the magnitude of the ozone change differs; in particular, our increase in ozone in SSP3.7-0 is lower as shown by Turnock et al. (2020). Moreover, our results for SSP3-7.0 do not show the strong decrease in ozone over the oceans as discussed by Zanis et al. (2022). Both differences can be expected, as we keep the methane lower boundary condition at present-day values and because we do not include the effects of changing meteorology and climate and therefore also have constant water vapour concentrations in all simulations (see Sect. 7 for a detailed discussion).

4.2 Land transport

Figure 3 shows the relative contributions of land transport emissions to ground-level ozone as simulated in the four experiments. In addition, the absolute contribution for 2015 and the changes in the absolute contribution for the various regions are shown as an average over specific regions in Fig. 4. These regions are Europe, North America, East Asia, South Asia, Southeast Asia, and South America (see Supplement Sect. S9.1 for a detailed definition). Additional figures depicting absolute contributions at ground level and zonal means are part of the Supplement (Sects. S3 and S4).

Generally, the absolute and relative contributions over North America, Europe, and the Middle East for present-day conditions (PD simulation) are comparable to previous studies (see Mertens et al., 2018, and detailed tables therein). The contributions for present-day conditions over India and parts of Southeast Asia, however, are larger compared to previous studies. This increase is mainly caused by the higher emissions in these regions in the Community Emissions Data System (CEDS) emission inventory compared to other emission inventories (e.g. Hoesly et al., 2018; McDuffie et al., 2020). Moreover, a more recent emission year (2015) has been used here.

For the SSP2-4.5 projection in 2050, the relative contributions of emissions from land transport to ground-level ozone ($C^{TRA}(O_3)$) at the hotspots over India and Southeast Asia increase to 30 % and 25 %, respectively (see Fig. 3). The absolute contributions increase over India, while they decrease over Southeast Asia (see Fig. 4), but due to the reduced ozone levels $C^{TRA}(O_3)$ increases. The increase over India is consistent with the increase in emissions from land transport in the SSP2 narrative, as the population grows fast and air pollution control strategies and technological development are

not strong enough to counteract the increased demand for mobility. Over Europe, East Asia, and North America, absolute and relative contributions of land transport emissions decrease due to stricter air pollution policies compared to the present day.

The SSP1-1.9 emission pathways show a strong reduction in land transport emissions in all regions of the world, which leads to a strong reduction in the contributions to ozone (see Fig. 3). The highest levels of $C^{TRA}(O_3)$ are simulated in the Middle East and South Asia (8 %–9 %). As O_3 itself decreases in SSP1-1.9 (see Fig. 2), absolute contributions decrease at an ever stronger pace (see Fig. 4). This strong decrease is caused by the strong shift in the transport system towards public transport and electrification of the transport system as well as the very strong air pollution mitigation efforts.

The SSP3-7.0 projection in 2050 globally features even higher land transport emissions compared to the present day, caused by the combination of population growth, slow technological development, and less strict air pollution mitigation. This increase in emissions globally leads to increasing contributions of the land transport emissions to ozone, but regional changes vary. Even though land transport NO$_x$ emissions are reduced by around 50 % compared to 2015 over North America and Europe, relative (16 %–18 %) and absolute contributions decrease only slightly. A detailed analysis of the reason will follow in Sect. 4.5. Over the Middle East, India, and South America $C^{TRA}(O_3)$ increases up to 28 %, 31 %, and 22 %, respectively. In these regions absolute contributions also increase. This increase is caused by an increase in emissions due to the combination of increased mobility demand, a lack of public transport, and the failure of effective emission control.

To quantify whether the changes in the contribution of land transport emissions to ground-level ozone for the future projections are caused by changes in regional emissions or by emission changes in other regions of the world, we performed a source–receptor analysis (see Figs. 5 and S18 in the Supplement). We define the tagged regions (see Table 1) as sources and the regions as used in Fig. 4 as receptor regions. Please note that the region of Southeast Asia is not defined as a separate source region but is listed under the rest of the world (ROW).

For all receptor regions in 2015, regional land transport emissions are the most important source for the contribution of land transport emissions to ozone. This means, for example, that land transport emissions from the source region of Europe contribute most to the contribution of land transport emissions to ozone in the receptor region of Europe. This changes in the projections for 2050, particularly for Europe and North America. Here, the contribution of regional land transport emissions declines sharply due to air pollution control and the source regions of the ROW have (partly) larger contributions compared to regional emissions.
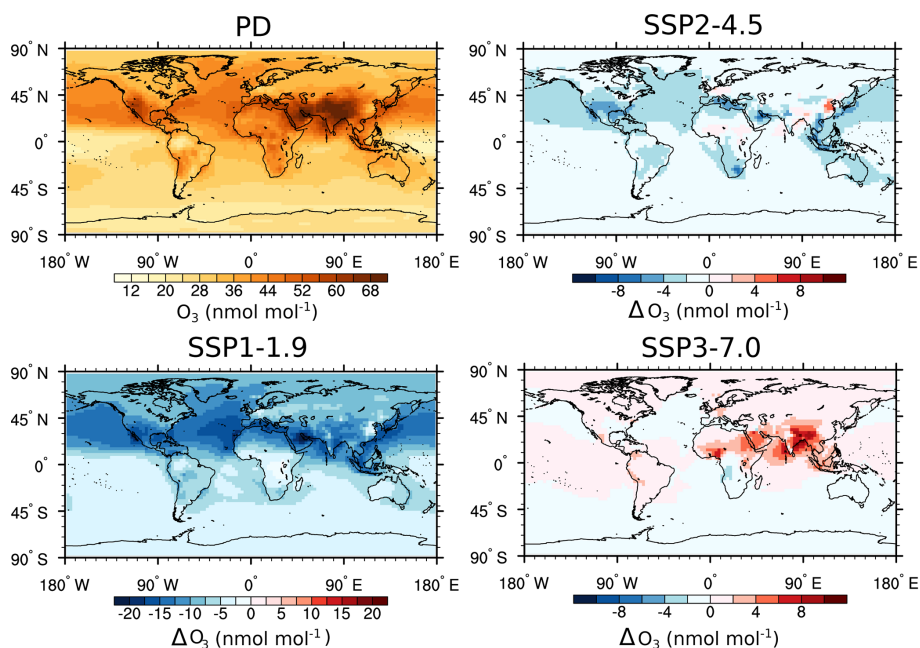
Figure 2. Ozone mixing ratios (5-year average) at ground level for the PD simulation and differences (ΔO_3, "2050 minus 2015") for SSP1-1.9, SSP2-4.5, and SSP3-7.0. Please note that SSP1-1.9 has a different colour scale.
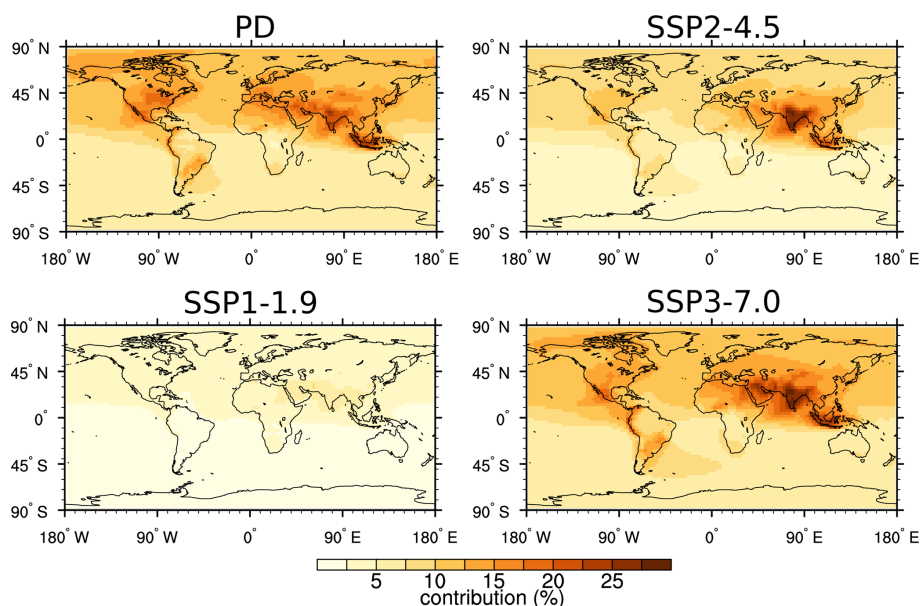

Figure 3. Relative contributions of land transport emissions to ground-level ozone (in %) for the simulations PD, SSP1-1.9, SSP2-4.5, and SSP3-7.0 (5-year average). The colour bars are identical in all panels to allow for better comparability between the results of the different emission projections.

Interestingly, only the emissions of the source regions of North America, South Asia, and East Asia have a larger influence on the contributions of land transport emissions for other receptor regions. The contributions of European land transport emissions to ground-level ozone are confined to

around Europe (see also additional figures in Sect. S3 in the Supplement).

The large contributions of land transport emissions for the present day and in the projections of SSP2-4.5 and SSP3-7.0, especially for South Asia, show the importance of strong mitigation measures in these regions to effectively reduce
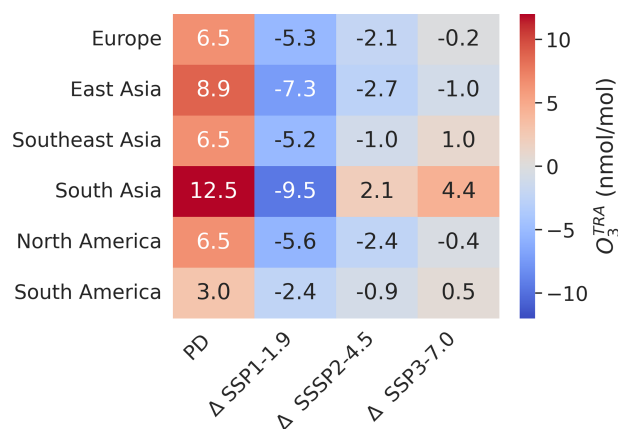
Figure 4. Absolute contributions of land transport emissions to ground-level ozone for 2015 and the differences in the absolute contributions for the three 2050 simulations (2050 minus 2015, all in $nmol\,mol^{-1}$). Values are area-averaged over specific geographical areas and for 5 years (see Sect. S9.1 in the Supplement for the exact definition of the regions).
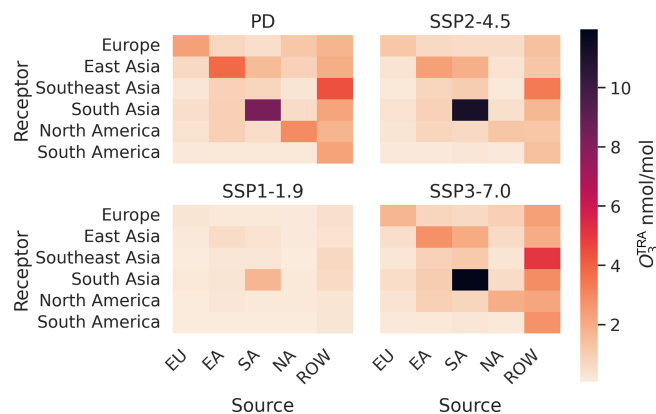

Figure 5. Source–receptor analysis of the absolute contribution of land transport emissions to ground-level ozone (in $nmol\,mol^{-1}$). The values are mean values over 5 years and area-weighted over the receptor regions. Exact definitions of the receptor regions are given in Sect. S9.1 in the Supplement.

O_3 levels. SSP1-1.9 shows one possible mitigation pathway, leading to a strong reduction in land transport emissions and its contribution to ozone over South Asia by strong shifts in the transport system and strong pollution control. In addition, the population increases less strongly, leading to a lower demand for mobility in SSP1-1.9 compared to SSP2-4.5 and SSP3-7.0 in South Asia.

Overall, the importance of regional emissions in most receptor regions indicates a large benefit for ground-level ozone when reducing regional emissions. However, the increasing importance of the contribution of land transport emissions from other regions in the projections shows how important it is to reduce ozone precursors not only regionally but also globally. In particular, the increase in the ROW contribution for Europe, South Asia, and North America in SSP3-7.0, in which international cooperation is strongly reduced, shows how important international cooperation is in order to reduce air pollution by long-range transport.

4.3 Shipping

Figure 6 shows the relative contributions of shipping emissions to ozone ($C^{SHP}(O_3)$) at ground level. Quantifications of the absolute contribution of shipping emissions for specific geographical regions, which are the Atlantic, Indian, and Pacific oceans and the Mediterranean Sea (see Sect. S9.2 in the Supplement for a detailed definition), are displayed in Fig. 7. Additional figures depicting absolute contributions at ground level and zonal means are part of the Supplement (Sects. S3 and S4).

Generally, $C^{SHP}(O_3)$ is largest in the northeastern Pacific and the northeastern Atlantic. In 2015, $C^{SHP}(O_3)$ reaches up to 18 % in these regions, corresponding to mixing ratios of

O_3^{SHP} of up to $7\,nmol\,mol^{-1}$ in the northeastern Pacific and up to $12\,nmol\,mol^{-1}$ along the western coast of North Africa. Similarly to the land transport emissions, the geographical distribution of shipping emissions for the present day is comparable to previous studies (Mertens et al., 2018; Butler et al., 2020). Despite higher emissions from the shipping sector, the simulated contributions in the present study are slightly lower compared to Mertens et al. (2018), which is probably due to the higher overall NO_x emissions in the present study. Compared to Butler et al. (2020), the simulated contributions in the present study are lower. This is due to the differences in the tagging methods used. While Butler et al. (2020) performed either NO_x or VOC tagging, we consider all precursors and their competition in ozone production and loss reactions simultaneously (see Sect. 7).

In contrast to the land transport sector, where the geographical patterns of the contributions change strongly due to the regional emission shifts resulting from the local nature of the mitigation measures in this sector, the geographical pattern of the regions with the largest contributions from the shipping sector remains very similar in 2050 for SSP2-4.5 and SSP3-7.0. This can be expected as the shipping emissions similarly do not show strong regional shifts (besides the introduction of SECAs) and mitigation measures are mostly applied globally due to technological advancements by means of improved emission factors (i.e. technological advancements). The absolute and relative contributions decrease to around 16 % ($8\,nmol\,mol^{-1}$) for SSP2-4.5 and 14 % ($7\,nmol\,mol^{-1}$) for SSP3-7.0. The lower contributions of shipping emissions in SSP3-7.0 compared to SSP2-4.5 are in accordance with lower shipping emissions caused by the decrease in global trade in the SSP3 narrative (see Sect. 3). The strong decrease in shipping emissions in SSP1-1.9 leads to a strong reduction in the absolute and relative contributions from shipping emissions to ozone. Ac-
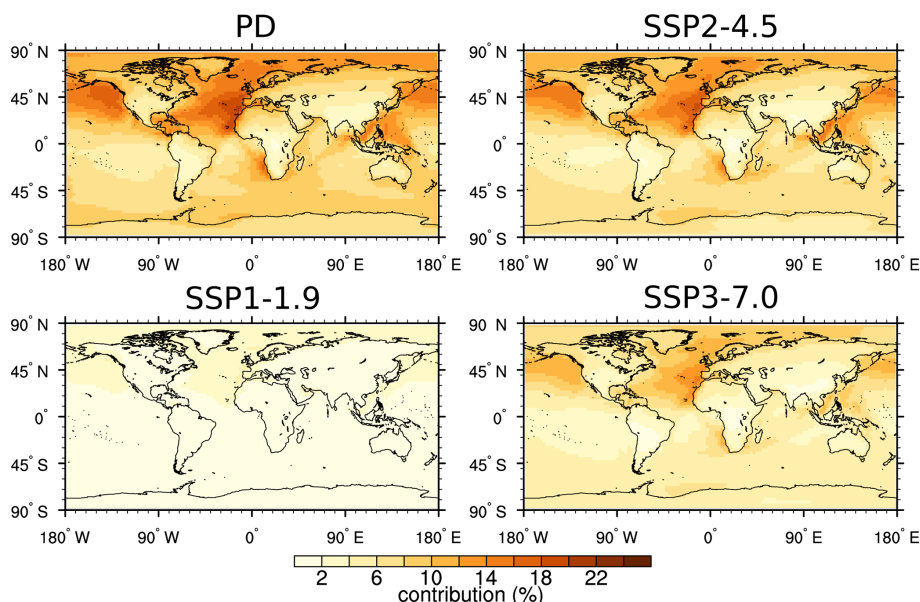
Figure 6. Relative contributions (in %) of shipping emissions to ground-level ozone as simulated by PD, SSP1-1.9, SSP2-4.5, and SSP3-7.0. All values are annual averages for the 5-year average. The colour bars are identical in all panels to allow for better comparability between the results of the different emission projections.
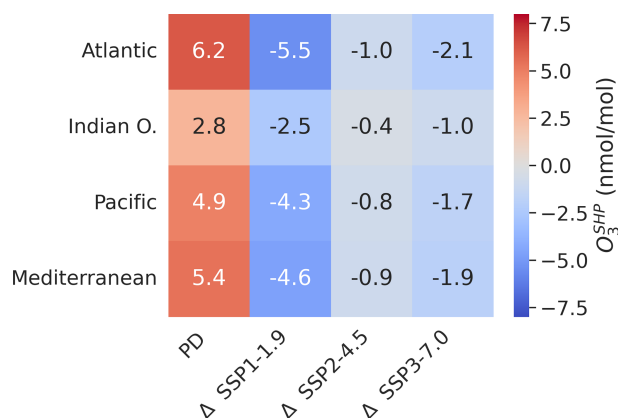

Figure 7. The 5-year mean of the absolute contributions of shipping emissions to ground-level ozone for PD and the differences in the absolute contributions for the three 2050 simulations (2050 minus 2015, all in $nmol\,mol^{-1}$). Values are area-averaged for specific geographical regions (see Sect. S9.2 in the Supplement for a detailed definition).

cordingly, $C^{SHP}(O_3)$ drops below 4 % and O_3^{SHP} drops to $2\,nmol\,mol^{-1}$ at its maximum. If climate change would be considered in addition, the ozone contribution from shipping emissions could be reduced even more strongly in the future, given the likely reduction in ozone over the oceans due to increasing humidity (Zanis et al., 2022; see also the discussion in Sect. 7).

4.4   Aviation

Figure 8 shows the zonal average of the relative contributions of aviation emissions to ozone ($C^{AIR}(O_3)$). Absolute contributions of aviation emissions to the tropospheric column of O_3^{AIR} averaged over the main flight regions between North America and Asia, Asia and Europe, and North America and Europe (see Sect. S9.3 in the Supplement for a detailed definition) are given in Fig. 9.

The largest values of the relative and absolute contributions in 2015 are simulated in the Northern Hemisphere. They reach up to 5 % (4–$5\,nmol\,mol^{-1}$) and occur over a large region between 60°–90° N (see Fig. S10 in the Supplement). The largest relative contributions can be found between 800 and 300 hPa, while the largest absolute contributions are simulated around 250 hPa. Generally, the geographical distribution of the regions with the largest contributions is similar to that of the regions with the largest ozone changes as quantified with the perturbation approach reported by Koffi et al. (2010). The results of the perturbation approach, however, show a relative change in ozone which is much more limited to the upper troposphere. This is because below the cruise altitude ozone precursors from other sources become more and more important. While in the perturbation approach the non-linearities in the net ozone production lead to a compensation of reduced emissions and increased net ozone production, here such a compensation is avoided.

The increase in the aviation emissions in SSP2-4.5 and SSP3-7.0 due to the increase in passenger travel demand leads to an increase in the ozone contributions. For the SSP2-4.5 projection, $C^{AIR}(O_3)$ reaches up to 10 % (8–
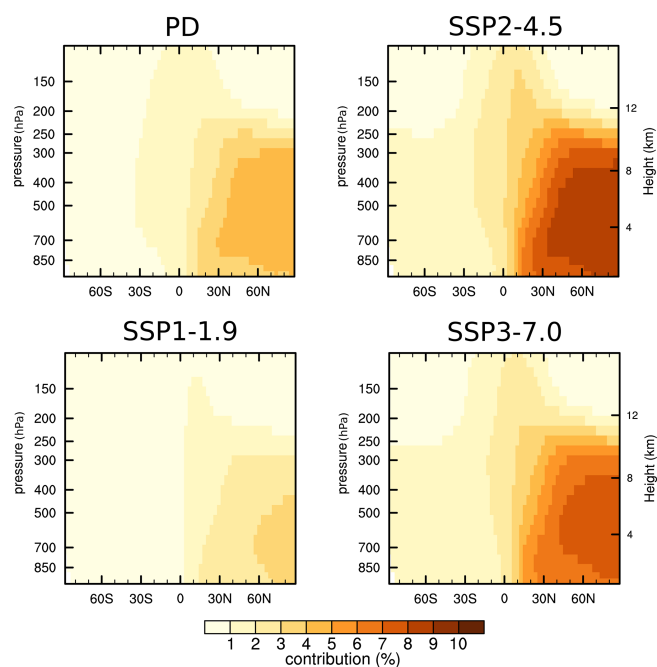
Figure 8. Zonal average of the relative contributions (in %) of aviation emissions to ozone as simulated by PD, SSP1-1.9, SSP2-4.5, and SSP3-7.0. All values are averages for 5 years. The colour bars are identical in all panels to allow for better comparability between the results of the different emission projections.

Figure 9. The 5-year mean tropospheric O_3^{AIR} column for PD (in Dobson units, DU) and the differences in the tropospheric O_3^{AIR} columns between the three 2050 simulations (2050 minus 2015). The values are area-averaged over the main flight regions (see Sect. S9.3 in the Supplement for a detailed definition).

$8.5\,\mathrm{nmol\,mol^{-1}}$) in the Northern Hemisphere in 2050. Like for the shipping emissions, the aviation emissions are lower in the SSP3-7.0 emission pathway compared to the SSP2-4.5 pathway. Accordingly, maximum relative and absolute contributions of aviation emissions to ozone reach up to $8\,\%$ (7–$7.5\,\mathrm{nmol\,mol^{-1}}$) in SSP3-7.0 for 2050. Similar to the absolute and relative contributions, the tropospheric ozone columns of O_3^{AIR} increase by almost $90\,\%$ (SSP2-4.5) and $70\,\%$ (SSP3-7.0) compared to present-day conditions (Fig. 9).

The SSP1-1.9 projection shows the lowest contributions in 2050 compared to the two other pathways, caused by decreased passenger travel demand compared to SSP2-4.5 and SSP3-7.0 and technological advancements compared to 2015. The maximum of $C^{AIR}(O_3)$ of around $4\,\%$ is only a slight reduction compared to the values in 2015. However, the background ozone is much lower in SSP1-1.9 for 2050 due to the overall decreased emissions so that the $4\,\%$ relative contribution corresponds to maximum absolute contributions of $2.5\,\mathrm{nmol\,mol^{-1}}$. Accordingly, the tropospheric ozone column of O_3^{AIR} also decreases by around $50\,\%$ in SSP1-1.9 compared to the present day.

4.5 Analysis of the non-linearity of the ozone chemistry

The production of tropospheric ozone is strongly non-linear and depends on the ratio of NO_x to VOC concentrations (e.g.
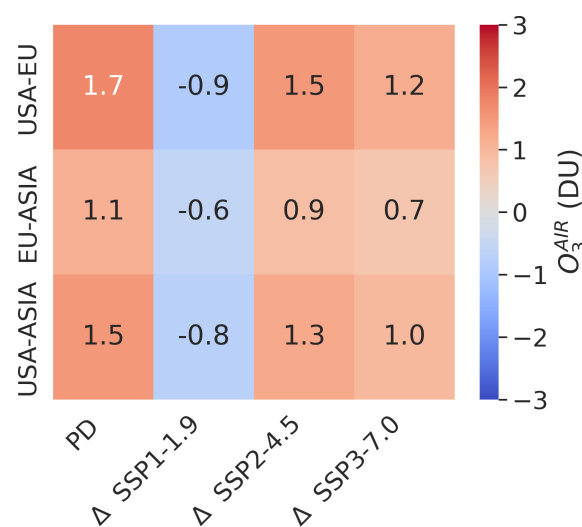
Sillman, 1995; Seinfeld and Pandis, 2006; Wu et al., 2009; Wild et al., 2012; Archibald et al., 2020). In the NO_x-limited regime, the ozone production efficiency (i.e. the number of ozone molecules formed by one NO_x molecule) increases if NO_x emissions are reduced and decreases with an increase in the NO_x emissions.

To analyse how the ozone burden in the atmosphere changes for the different projections, we introduce the following metric which we define exemplary for the shipping sector as follows:

$$\chi^{SHP} = \frac{B(O_3^{SHP})}{E(NO_x^{SHP})}. \tag{3}$$

In this definition, $B(O_3^{SHP})$ is the global burden (in Tg) of O_3^{SHP} and $E(NO_x^{SHP})$ is the annual NO_x emissions of the shipping sector (in Tg (NO)). Increasing values of χ (called the ozone burden efficiency) indicate an increase in the ozone burden per emitted NO_x. We prefer this quantity over the commonly analysed ozone production efficiency as it includes production and loss processes of ozone and therefore is a better measure of the associated radiative forcing.

Figure 10 shows the dependency between χ and the NO_x emissions. The results clearly show the expected increase in the ozone burden efficiency with decreasing emissions. Depending on the prevailing meteorological conditions and on the chemical background conditions, χ varies among the transport sectors and in different world regions (as analysed for the land transport emissions). Generally, NO_x emissions from the aviation sector have a larger efficiency in forming ozone compared to surface emissions because the emissions are emitted under cleaner background conditions. This
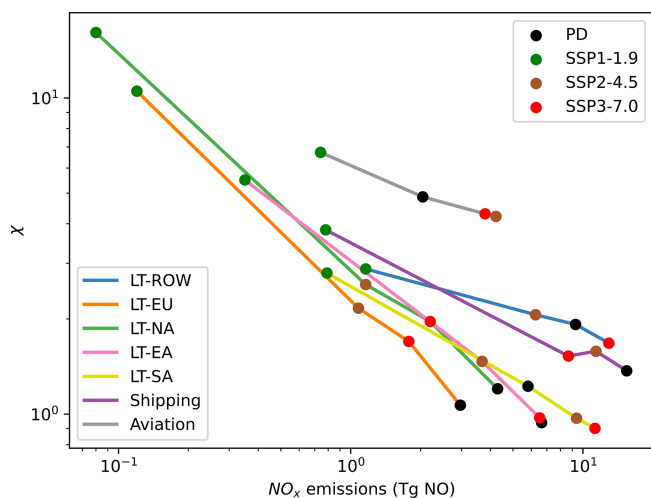
Figure 10. Dependency between χ and the annual NO_x emissions (in Tg (NO)). χ is calculated as the global mean over 5 years. Shown are the results of the seven transport categories (LT-ROW, LT-EU, LT-NA, LT-SA, LT-EA, aviation, and shipping, where LT indicates land transport) for each simulation (colour-coded).

is consistent with previous findings (e.g. Hauglustaine et al., 1994; Derwent et al., 2001; Hoor et al., 2009; Dahlmann et al., 2011; Butler et al., 2020; Wang et al., 2022; Terrenoire et al., 2022). Land transport emissions in Europe or North America have rather low values of χ (at least) for the present day, as they are emitted in a rather polluted background and the prevailing meteorological conditions do not favour ozone production over parts of North America and Europe. This is in agreement with the results of Zhang et al. (2016), showing a larger ozone production efficiency near tropical regions compared to mid-latitudes.

The increase in χ with decreasing NO_x emissions underlines a major challenge for ozone mitigation. A very prominent example is the land transport emissions from Europe and North America in SSP3-7.0. Even though the NO_x emissions are reduced by around 40 % (Europe) and 50 % (North America) compared to 2015, the global burden of ozone produced from these emissions is reduced by 5 % (Europe) and 16 % (North America), only. Accordingly, reductions in NO_x emissions from the land transport need to be large enough to overcome strong non-linear behaviour of the ozone chemistry so that the emission reductions lead to significant reductions in ozone. The SSP1-1.9 and SSP2-4.5 projections show two possible projections with such strong reductions over Europe and North America. As an example, the reduction in NO_x emissions of 63 % over Europe in SSP2-4.5 compared to 2015 leads to a 30 % reduction in ozone from European land transport emissions.

5 Ozone radiative forcing

The stratospherically adjusted radiative forcing of ozone (for simplicity from now on called RF) of the different transport sectors is depicted in Fig. 11. RF values are given for the three main transport sectors (Fig. 11a) and for the land transport emissions from specific regions in Fig. 11b (see Table 1 for the naming convention). The total RF of the land transport sector in 2015 is 121 mW m^{-2}. This value is 29 mW m^{-2} (≈ 32 %) larger compared to Mertens et al. (2018), which is partly due to the ~ 35 % higher NO_x emissions from land transport in the present study. Moreover, especially the land transport emissions in Asia are larger in the present study, which have a rather high efficiency for RF (see Sect. 5.1).

The RF of the shipping sector in 2015 is 54 mW m^{-2}, which is 8 mW m^{-2} (≈ 13 %) lower compared to Mertens et al. (2018), despite the about 20 % higher NO_x emissions in the present study. This is most likely caused by the overall higher NO_x emissions from anthropogenic sources in the present study compared to Mertens et al. (2018). These higher overall NO_x emissions lead to a more polluted background and a lower ratio of the shipping emissions compared to all anthropogenic emissions (around 7 % in the present study compared to 12 %).

The RF of the aviation sector in 2015 is 29 mW m^{-2}, which lies between the best estimates by Lee et al. (2021) for 2011 (27 mW m^{-2}) and 2018 (36 mW m^{-2}). Note that the values from Lee et al. (2021) are based on a literature review from various models using the perturbation approach. Only a limited number of model results from EMAC are included in the multi-model assessment. The included results of EMAC tend to be at the lower end of the ozone response in Lee et al. (2021) and also in other multi-model assessments (Søvde et al., 2014; Cohen et al., 2023). A recent assessment with EMAC, comparing different methodologies to assess the effects of aviation emissions on ozone, diagnoses a difference in ozone between the perturbation and tagging method of a factor of 1.16 to 2.55, with a mean value of 1.83 (Maruhashi et al., 2024).

As mentioned in Sect. 3, inconsistent geographical distributions in the CMIP6 aviation emissions applied here lead to an underestimation of the aviation O_3 RF of about 8 % (see Thor et al., 2023, for a detailed analysis).

The RF from land transport emissions is reduced to 103 mW m^{-2} in 2050 with the SSP2-4.5 projection. The strong increase in the emissions from the land transport sector in SA leads to an increase in the RF from O_3^{LT-SA} compared to 2015 of around 7 mW m^{-2}. The RF of the land transport emissions of all other regions decreases slightly. The RF of the shipping emissions decreases slightly by 2 mW m^{-2} in 2050 compared to 2015, while the RF of the aviation sector almost doubles with SSP2-4.5. With this large increase, the RF of the aviation sector is slightly larger than the RF of the shipping sector in 2050 for SSP2-4.5. Moreover, the RF of the total transport sector (land, aviation, and shipping) in

2050 with the SSP2-4.5 projection is almost as large as for present-day conditions, as the increase in the RF in the aviation is almost of the same magnitude as the reductions in shipping and land transport.

The strong increase in the land transport emissions in SSP3-7.0 compared to SSP2-4.5 leads to an increase in the RF from land transport emissions to $140 \, \text{mW m}^{-2}$ in 2050. In comparison to 2015 and to SSP2-4.5 (in 2050) especially the RF of the land transport emissions increases from the rest of the world (ROW). Also the contributions of land transport emissions from South Asia increase mainly due to the strong increase in the emissions in India. The RF of the land transport emissions from Europe, North America, and East Asia stay relatively similar to 2015. Even though the NO_x emissions from land transport are reduced strongly, ozone is only reduced slightly due to non-linear effects (see Sect. 4.5).

Consistent with the changes in NO_x emissions and the O_3 contributions, RF from the aviation and shipping sectors is smaller for SSP3-7.0 compared to SSP2-4.5. The RF from shipping emissions is $37 \, \text{mW m}^{-2}$ in 2050 with SSP3-7.0, which is a decrease of 17 and $15 \, \text{mW m}^{-2}$ compared to SSP2-4.5 in 2015 and 2050, respectively. The RF from aviation emissions decreases for SSP3-7.0 by $5 \, \text{mW m}^{-2}$ compared to SSP2-4.5 in 2050 but increases by $21 \, \text{mW m}^{-2}$ compared to 2015.

In the SSP1-1.9 projection, RF from all transport sectors decreases strongly. The total land transport RF is reduced by a factor of 4, the shipping RF is reduced by a factor of 5, and the RF from aviation emissions is reduced by a factor of 3 compared to 2015. Also the RF of the land transport emissions from various regions is reduced strongly compared to 2015 and also compared to the other projections.

5.1 Radiative forcing efficiency

The RF values discussed in Sect. 5 are difficult to compare among the different sectors due to the different amount of emissions for each sector and region. To put the discussed RF values into perspective with the emissions of the individual emission sectors, we calculate the RF efficiency with respect to the NO_x emissions for each sector (defined as RF_e, e.g. Dahlmann et al., 2011) as

$$RF_e^i = \frac{RF^i}{E(NO_x^i)}, \tag{4}$$

with $E(NO_x^i)$ denoting the NO_x emissions (in $\text{Tg}(\text{NO})\,\text{a}^{-1}$) and RF^i denoting the stratospherically adjusted RF of the considered sector (denoted as i). In addition, we calculate the RF with respect to the tropospheric ozone columns, denoted as $O3_{tc}$, in Dobson units (DU), for each emission sector (denoted as i). We call this quantity RF_{DU} and define it as

$$RF_{DU}^i = \frac{RF^i}{O3_{tc}^i}. \tag{5}$$

Figure 12 shows RF_e and RF_{DU} for the different projections and the different emission sectors. For the present day, the aviation sector has the largest RF_e value of $15.2 \, \text{mW m}^{-2}(\text{Tg}(\text{NO})\,\text{a}^{-1})^{-1}$ $(32.5 \, \text{mW m}^{-2}(\text{Tg}(\text{N})\,\text{a}^{-1})^{-1})$. This is in general in line with previous studies (e.g. Hauglustaine et al., 1994; Derwent et al., 2001; Hoor et al., 2009; Butler et al., 2020; Terrenoire et al., 2022) and the high ozone burden efficiency from aviation NO_x emissions discussed in Sect. 4.5. Moreover, the value is 30 % $(7.5 \, \text{mW m}^{-2}(\text{Tg}(\text{N})\,\text{a}^{-1})^{-1})$ larger than the multi-model mean of $25.1 \pm 7.3 \, \text{mW m}^{-2}(\text{Tg}(\text{N})\,\text{a}^{-1})^{-1}$ by Lee et al. (2021) (see also discussion in Sect. 5). The inclusion of the correction of the CMIP6 aviation emissions as reported by Thor et al. (2023) increases the efficiency to $16.3 \, \text{mW m}^{-2}(\text{Tg}(\text{NO})\,\text{a}^{-1})^{-1}$ $(34.9 \, \text{mW m}^{-2}(\text{Tg}(\text{N})\,\text{a}^{-1})^{-1})$.

RF_e for shipping is slightly smaller than for total land transport emissions, caused by the much more effective upward transport of land transport emissions by convection into the upper troposphere compared to shipping emissions as already discussed by Hoor et al. (2009) (see also zonal means in Sect. S4 in the Supplement). Land transport emissions from East Asia, Europe, and North America show the smallest RF_e values because ozone is formed rather inefficiently from emissions of these regions (see Sect. 4.5). Moreover, especially for Europe and North America, the produced ozone is not transported into the upper troposphere very efficiently where it would be most radiatively active (e.g. Riese et al., 2012; Rap et al., 2015). The latter is analysed using RF_{DU}, which is largest for land transport emissions from South Asia. This is in agreement with results from Dahlmann et al. (2011) reporting a strong latitude dependence of RF_{DU} with the highest values near the Equator. Even though aviation has the largest RF_e values, RF_{DU} is lower as most emissions take place in mid-latitudes to high latitudes (Dahlmann et al., 2011).

In the future projections, RF_e increases for those emission sectors and regions whose emissions decrease and RF_e decreases where the emissions increase. The change in RF_e agrees with the change in χ. The large values of RF_e for some sectors with SSP1-1.9 emissions are partly also dominated by the small amount of emissions, leading to numerical difficulties in calculating the quotients.

The strong decrease in the emissions in the SSP1-1.9 projections leads to an increase in RF_{DU}, caused by reduced saturation effects of the radiative efficiency as analysed by Dahlmann et al. (2011). This increase in the radiative efficiency causes an additional penalty on ozone mitigation, as ozone gets more radiatively efficient if tropospheric ozone levels are strongly reduced.
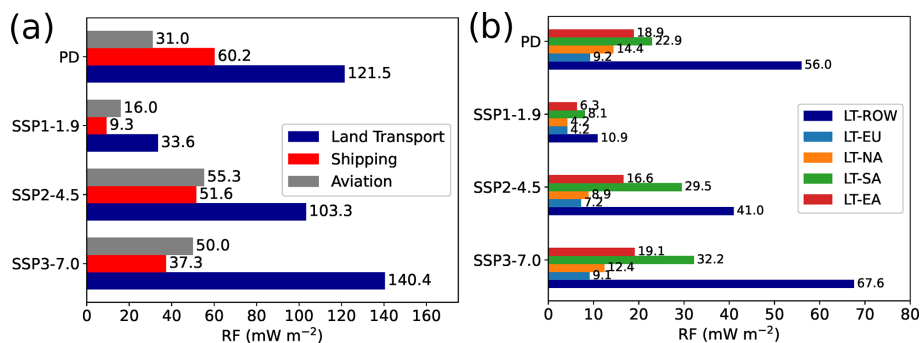
Figure 11. Stratospheric adjusted radiative forcing of ozone (in mW m^{-2}) from each sector (a) and for land transport emissions from specific regions (b).
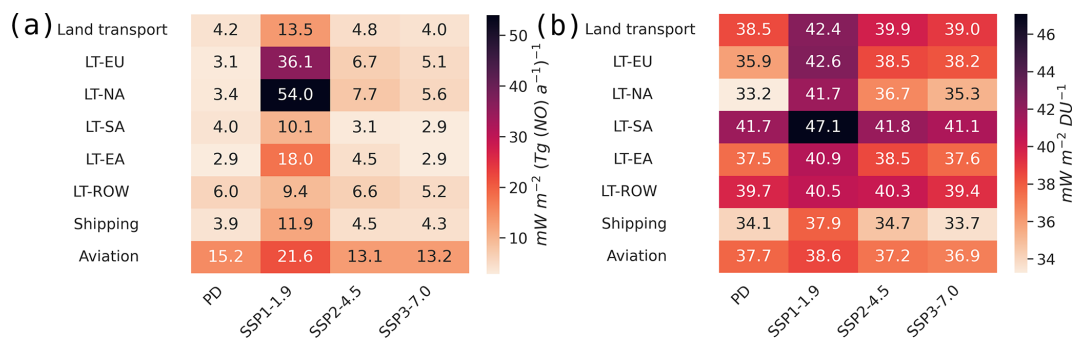

Figure 12. Global averages of RF$_e$ (a, in mW m^{-2}((Tg (NO) a^{-1})$^{-1}$)) and RF$_{DU}$ (b, in mW m^{-2} DU^{-1}) for the emission sectors land transport, shipping, and aviation as well as for the land transport emissions from specific regions only.

6 Contributions of transport emissions to OH and to the methane lifetime

Emissions of the transport sector not only affect tropospheric ozone levels but also have a strong influence on OH mixing ratios and with this on the tropospheric oxidation capacity. Increases in OH lead to a reduction in the methane lifetime. Previous studies analysed the influence of transport emissions on OH and methane lifetime with the perturbation approach (e.g. Hoor et al., 2009). Here, we determine the contribution of the emissions from the transport sector to OH and the associated contributions to the methane lifetime for the first time with a source attribution method. Due to the methodological differences, the results obtained in the present study are not directly comparable to previous studies. Therefore, we also performed three perturbation simulations, in which we applied a 5 % emission reduction to land transport, shipping, and aviation, respectively. The changes in the methane lifetime by emissions from land transport, aviation, and shipping with this method are in agreement with Hoor et al. (2009), who applied the same 5 % perturbation (see Sect. S5 in the Supplement).

6.1 Contributions to OH

Figure 13 depicts the zonal average of the contribution of land transport emissions to OH (OH^{TRA}). The zonal mean pattern of the contribution for the present-day simulation is similar than the one presented by Rieger et al. (2018). Two maxima of OH^{TRA} appear, one in the lower troposphere between the surface and 600 hPa at 0–30° N peaking at 20 fmol mol^{-1} and one in the upper tropical troposphere between 100 and 200 hPa peaking at 26 fmol mol^{-1}. The maximum in the upper troposphere, however, is mainly due to the overall very large OH mixing ratio in these regions, and the relative contributions in these regions are rather low (up to 5 % in 2015). Near the surface, the relative contributions of land transport emissions to OH reach up to 40 % in the Northern Hemisphere in 2015. Hoor et al. (2009) reported only one maximum in the lower troposphere by applying the perturbation approach. This corroborates the fact that results of the attribution method and of the perturbation methods are not directly comparable. This second maximum of OH^{TRA} is caused by photolysis of O$_3^{TRA}$ in the upper troposphere and subsequent formation of OH.

Due to the strong interconnection between NO$_x$, O$_3$, and OH in atmospheric chemistry, the overall changes in OH^{TRA} in the future projections are similar to those discussed for the O$_3$ contributions in Sect. 4.2. Accordingly, increases in
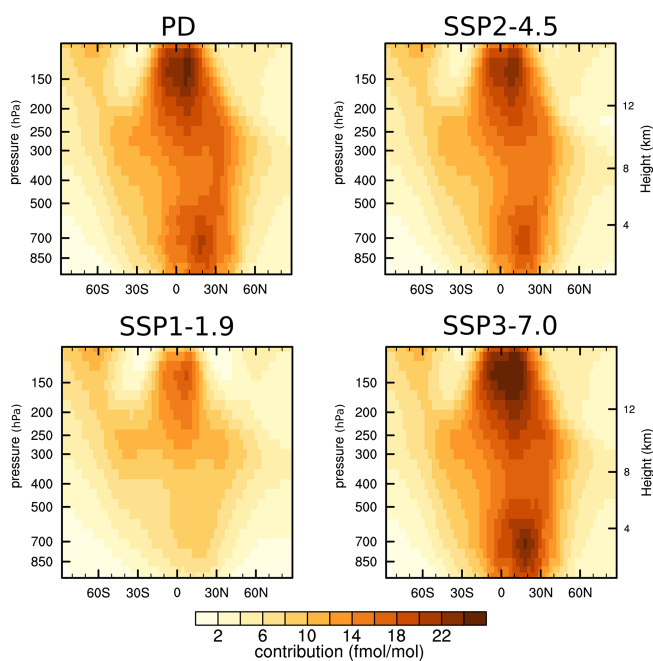
Figure 13. Zonal average of the absolute contribution of land transport emissions to OH (in $fmol\,mol^{-1}$) for PD, SSP1-1.9, SSP2-4.5, and SSP3-7.0. The values shown are 5-year averages.
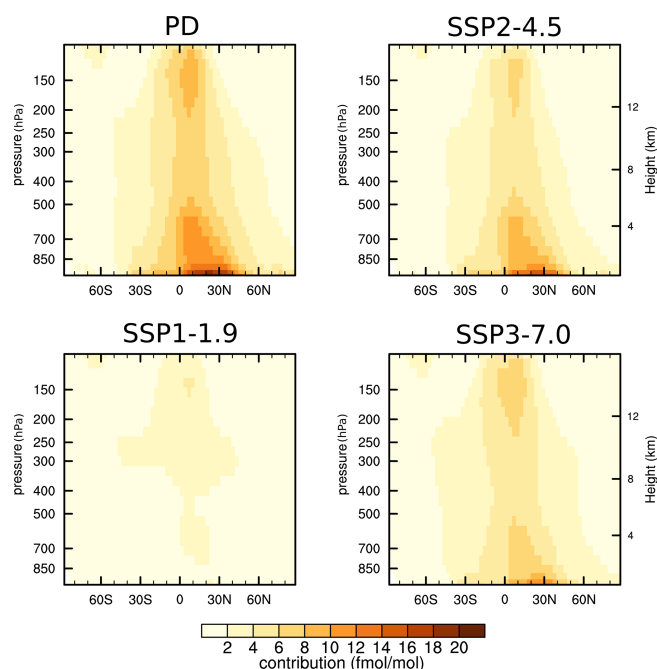

Figure 14. Zonal average of the absolute contribution of shipping emissions to OH (in $fmol\,mol^{-1}$) for PD, SSP1-1.9, SSP2-4.5, and SSP3-7.0. The values shown are 5-year averages.

the NO_x emissions from land transport lead to an increase in OH^{TRA} and vice versa. Besides the changes in NO_x, changes in the VOC or CO emissions will also affect OH. Contributions of land transport emissions to CO and VOC are, however, not analysed in detail in the present study because it is beyond the scope of the present study.

As for O_3^{SHP}, OH^{SHP} is mainly limited to the lower troposphere (see Fig. 14). The maxima are simulated near the surface, with enhanced contributions up to 500 hPa. In the tropical upper troposphere only small contributions are simulated because O_3^{SHP} is also limited to the lower troposphere (see Sect. S3 in the Supplement). In 2015, the zonal average of OH^{SHP} reaches up to $16\,fmol\,mol^{-1}$ near the surface and decreases to 8–$12\,fmol\,mol^{-1}$ in the middle and upper troposphere.

In accordance with the changes in the emissions in the three SSP projections, the contributions of OH^{SHP} are lowest in SSP1-1.9, followed by SSP3-7.0 and SSP2-4.5, which has the largest contributions in 2050. The contributions in 2050 with SSP2-4.5 emissions, however, are lower compared to 2015.

The zonal average of OH^{AIR} (see Fig. 15) shows a clear peak in the Northern Hemisphere between 30–60° N and 200–300 hPa, which is in accordance with Rieger et al. (2018). The region with the maxima of OH^{AIR} is similar to the region of the largest impact of aviation emissions on OH at around 40° N and between 200–300 hPa reported by Hoor et al. (2009). In 2015 the zonal average of OH^{AIR} peaks up to $22\,fmol\,mol^{-1}$. In agreement with the changes in the aviation

emissions and O_3^{AIR}, OH^{AIR} increases in 2050 for SSP2-4.5 (up to $36\,fmol\,mol^{-1}$) and SSP3-7.0 (up to $33\,fmol\,mol^{-1}$) compared to 2015. Due to the large decrease in emissions in SSP1-1.9, peak values of the zonal average of OH^{AIR} decrease to $13\,fmol\,mol^{-1}$.

As OH is strongly coupled to O_3 (and vice versa), OH also shows a non-linearity similar to O_3. Accordingly, the OH contributions also respond non-linearly to the changes in the emissions from the traffic sectors (see Sect. S7 in the Supplement).

6.2 Reductions in the methane lifetime

Methane is an important greenhouse gas and therefore changes in its lifetime, e.g. due to changes in OH caused by emissions of the transport sector, might contribute significantly to the climate effect of transport emissions. Based on the contributions of the different emission sectors to OH, the effect of the different emission source on the methane lifetime is analysed. This analysis helps us to understand how the transport emissions affect the methane lifetime. In the following we define methane lifetime as the yearly global mean of CH_4 divided by the yearly global mean (expressed as overbars) of the loss of CH_4 by OH as diagnosed by TAGGING (loss$(CH_4)_{total}$; see Rieger et al., 2018):

$$\tau(CH_4) = \frac{\overline{CH_4}}{\overline{loss(CH_4)_{total}}}. \tag{6}$$
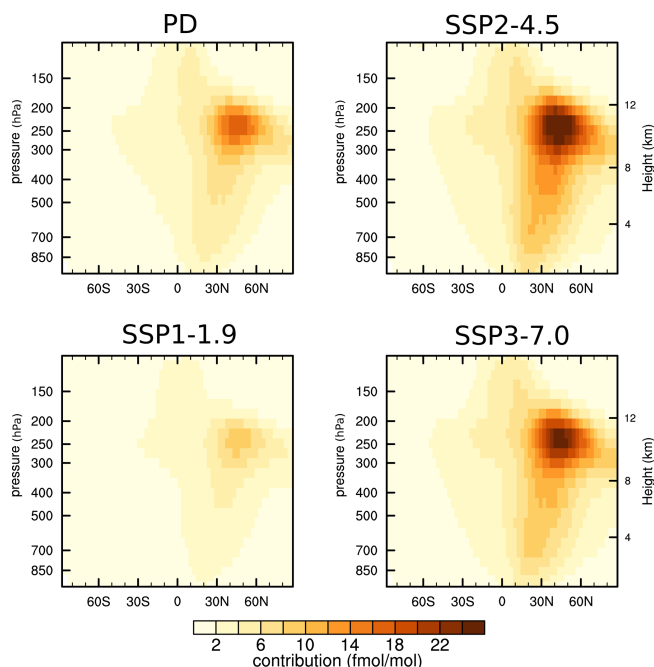
Figure 15. Zonal average of the absolute contribution of aviation emissions to OH (in $fmol\,mol^{-1}$) for PD, SSP1-1.9, SSP2-4.5, and SSP3-7.0. The values shown are 5-year averages.

The lifetime is calculated for the troposphere, i.e. below the monthly-mean tropopause (pressure) height. In the present study the tropopause is defined according to the World Meteorological Organization (WMO) definition based on the temperature lapse rate for latitudes equatorward of 30° and as the potential vorticity iso-surface of 3.5 PVU (potential vorticity unit) at latitudes poleward of 30° (see Grewe and Dameris, 1996, for an analysis on the effects of different tropopause definitions).

The loss rates of CH_4 for 18 different sectors, including the transportation sectors land, ship, and aviation, are diagnosed based on the OH contribution discussed in Sect. 6.1. Based on these OH contributions, the relative reduction in the methane lifetime of a specific emission source (for example shipping emissions) is then calculated as

$$\Delta_{rel}\tau(CH_4)_{SHP} = \frac{\overline{\tau(CH_4)}_{total} - \overline{\tau(CH_4)}_{no-SHP}}{\overline{\tau(CH_4)}_{no-SHP}}$$

$$= -\frac{\overline{loss(CH_4)}_{SHP}}{\overline{loss(CH_4)}_{total}}, \qquad (7)$$

where "SHP" is the CH_4 loss attributed to the emissions of the shipping sector based on OH^{SHP} and "no-SHP" is the loss of all other categories, excluding the shipping sector. Please note that the reciprocals of the methane lifetime calculated for each tagged OH are additive and sum up to the total methane lifetime as calculated by Eq. (6). The relative reduction as calculated according to Eq. (7) always refers to the total methane loss for one specific simulation. Thus,

the relative reduction in the methane lifetime for one simulation sums up to 100 %. In the different simulations, the methane lifetime differs slightly. This needs to be considered when comparing the relative reductions in the methane lifetime analysed for the different simulations. The methane lifetimes analysed for the different simulations by Eq. (6) are 7.46 a (2015), 7.45 a (SSP2-4.5 in 2050), 7.43 a (SSP3-7.0 in 2050), and 8.01 a (SSP1-1.9 in 2050).

Figure 16a shows the relative reduction in the methane lifetime (calculated with Eq. 7) due to the emissions of the different transport sectors for 2015 and the three emission projections in 2050. Generally, transport emissions lead to a reduction in the methane lifetime and hence to a reduction in the climate effects of methane. From all transport modes, the land transport emissions have the largest effect on the methane lifetime. The relative reductions in the methane lifetime by land transport emissions ($\Delta_{rel}\tau(CH_4)_{TRA}$) range between -7 % (SSP1-1.9) and -16 % (SSP3-7.0). The relative reductions in the methane lifetime from shipping emissions ($\Delta_{rel}\tau(CH_4)_{SHP}$) range from -9 % (PD) to -2 % (SSP1-1.9). The relative reductions in the methane lifetime of aviation emissions ($\Delta_{rel}\tau(CH_4)_{AIR}$) are lowest for SSP1-1.9 (-3 %) and largest for SSP2-4.5 (-7 %) and SSP3-7.0 (-6 %) emissions. Despite the 2015 conditions, shipping and aviation have similar relative reductions in the methane lifetime, even though the shipping sector has much higher emissions (see Fig. 1). This is due to the larger mixing ratios of OH^{AIR} compared to OH^{SHP} (see Sect. 6.1). Moreover, due to the strong non-linearity of the OH chemistry, even in the clean SSP1-1.9 projection the transport sectors, especially the land transport sector, have a rather large effect on the methane lifetime. This non-linearity is larger for the reduction in the methane lifetime than for the ozone RF. As an example, the ozone RF of land transport decreased by around 70 % between 2015 and SSP1-1.9, while the relative reduction in the methane lifetime is 50 %. The reverse effect can be observed when increasing transport emissions; for example the ozone RF of land transport emissions between 2015 and SSP3-7.0 increases by 15 %, while the reduction in the methane lifetime changes by 8 %.

Figure 16b breaks down the reduction in the methane lifetime by land transport emissions to the different geographical regions. In agreement with the contributions to the ozone RF (see Sect. 5) the largest relative reduction in the methane lifetime is caused by land transport emissions from the rest of the world (LT-ROW). Relative reductions in the other regions are smaller by a factor of 2–3, with the largest relative reductions coming from South Asia (LT-SA).

Generally, the relative reductions in the methane lifetime as analysed by the source attribution approach are much larger than relative reductions in the methane lifetime calculated by a 5 % perturbation (see Sect. S5 in the Supplement for a detailed analysis for 2015 conditions). The reduction in the methane lifetime as analysed by the perturbation approach is -1.9 % for the land transport emissions,

−4.5 % for the shipping emissions, and −1.1 % for the aviation emissions, respectively. Accordingly, the reductions in the methane lifetime diagnosed by the source attribution approach are larger by a factor of 7.7 (land transport), 1.9 (shipping), and 3.5 (aviation) compared to the reductions as analysed by a 5 % reduction with the perturbation approach. This large difference in the relative reductions in the methane lifetime as analysed by the two methods also leads to shifts in the ranking of the different transport sectors with respect to the influence of the methane lifetime. While with the perturbation method the shipping emissions are larger by a factor of 2 compared to land transport emissions, with the source attribution method the contribution of land transport emissions is larger by a factor of 2 compared to shipping emissions. The main reason for this different behaviour is that most shipping emissions take place in cleaner environments with fewer emissions compared to the land transport emissions. In these cleaner environments the non-linearity of the ozone chemistry is not that pronounced and the linearization of the perturbation approach does not affect the results strongly (see also Grewe et al., 2010).

7 Limitations and uncertainties

In the following we discuss the limitations and uncertainties of this study. The main points we discuss are the usage of the same meteorological conditions and methane emissions in all simulations, the different available tagging methods for source attribution, and the influence of the errors in the geographical distribution of the aviation emissions in CMIP6.

7.1 Effects of climate change

The signals of emissions from specific regions or specific emission sources (e.g. from aviation) are small. To quantify these signals, we apply the QCTM mode (see Sect. 2), in which chemistry and dynamics are decoupled. Accordingly, the dynamics (and therefore the climatic state) is identical in every model simulation. This approach of applying present-day dynamics for future emission scenarios is commonly used when the effects of certain emission changes or sources on the atmospheric chemistry are investigated on the global and regional scale, e.g. Eyring et al. (2007), Hoor et al. (2009), Hodnebrog et al. (2012), Righi et al. (2015), and Matthias et al. (2016).

Due to this approach, however, our model simulations do not consider changes in meteorology and climate between 2015 and 2050. Accordingly, emissions which are based on meteorological conditions (e.g. biogenic emissions, lightning NO_x) are identical in all simulations. With climate change, these emissions are likely to increase (von Schneidemesser et al., 2015). This increase could alter the contributions of the anthropogenic emissions; for instance increased biogenic VOC emissions may affect the ozone production efficiency,

while increased lightning NO_x in the upper troposphere may compete with NO_x emissions from the aviation sector.

Moreover, increased biogenic emissions and changed atmospheric conditions (e.g. increased temperature and its effects on kinetics) likely lead to an increase in ozone near highly polluted regions (known as a "climate penalty", Zanis et al., 2022). In addition, climate change likely leads to a decrease in ozone in remote regions due to the increase in water vapour (known as a "climate benefit", Zanis et al., 2022). In addition, during periods of droughts and heat waves, reduced ozone deposition to vegetation could increase ground-level ozone (Lin et al., 2020).

Altogether, this could also affect the contributions of the traffic emissions. A reduced lifetime of ozone, especially over the oceans, would likely lead to a reduction in ozone attributable to shipping emissions. Long-range transport, especially the source–receptor relationships, might also be affected by changes in the ozone lifetime. At the same time, the increase in ozone in polluted regions in a changing climate could affect ozone contributions especially from land transport emissions.

Koffi et al. (2010) considered the effects of climate change on the ozone effects of transport emissions, applying a 5 % emission reduction (i.e. with the perturbation approach). Globally, they report a small decrease in the ozone changes caused by transport emissions due to climate change but with strongly varying regional patterns. The effect of climate change on ozone contributions (i.e. applying a tagging approach) needs to be analysed in follow-up studies.

7.2 Land-use change

Similar to changes in the climate, changes in land use also affect ozone (e.g. Wu et al., 2012; Wang et al., 2020). The effects of land-use change on ozone are due to various processes, such as changes in biogenic emissions, effects on dry deposition, and changes in temperature (e.g. by effects on radiation and evapotranspiration). Land-use change, as well as the corresponding effects, also particularly depends on the considered scenario (Popp et al., 2017). These effects are not considered to isolate the effects of the emission changes only.

7.3 Fixed lower boundary condition for methane

To be able to estimate only the effect of the changing anthropogenic emissions of short-lived species, we also kept the lower boundary conditions for methane fixed in all model simulations. We chose this approach to be able to attribute and understand the effects of the changes in the other ozone precursors in more detail. Increasing methane levels strongly affect atmospheric chemistry. In addition, increasing methane levels can have very complex effects on ozone produced from a specific emission source. As an example, Butler et al. (2020) reported a strong increase in ozone attributable to shipping emissions with increasing methane levels, while
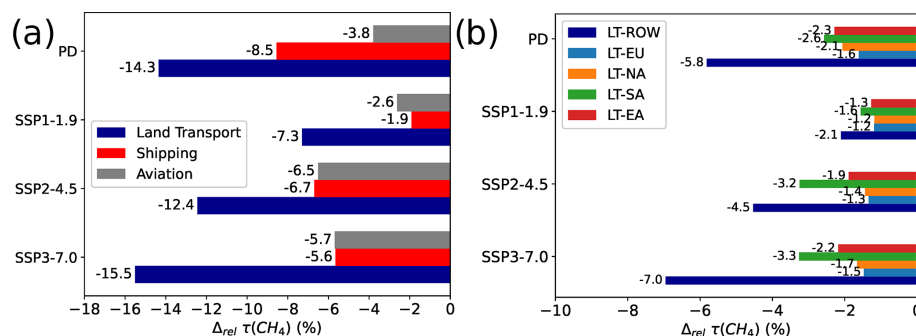
Figure 16. Methane lifetime reduction by different emission sectors based on their contributions to OH: for the sectors land, aviation, and shipping and for different SSPs **(a)** and for total transportation (all transport sectors) from different regions and for different SSPs **(b)**. Note that lifetime reductions due to individual sectors are additive. See the text for a description of the calculation. All values are 5-year averages.

the contribution of other emission sources showed a smaller increase. To suppress such complex effects, we kept the CH_4 lower boundary condition constant in all simulations. To investigate how increased methane levels would affect the results, we performed an additional sensitivity study for 2050, taking short-lived emissions and lower boundary conditions for methane from the SSP2-4.5 projection for 2050. In this simulation, globally averaged prescribed methane mixing ratios at the surface are around 9 % larger compared to the SSP2-4.5 simulation. This increase leads to a ≈ 2.5 % (or 0.9 DU) increase in globally averaged tropospheric ozone columns. Similar to those reported by Butler et al. (2020), the contributions show a very heterogeneous response. The contribution to tropospheric ozone of emission categories with strong NO_x emissions increases, with the largest increases by the categories lightning (3.7 %), N_2O degradation (3.1 %), aviation (2.9 %), and shipping (2.4 %). In addition, ozone attributed to methane degradation also increases by 9.1 % (see also Sect. S6 in the Supplement). Moreover, the response of the methane increase in our study differs from the results reported by Butler et al. (2020), which is caused by differences in the tagging approach (see the next paragraph) and by different emission inventories and different magnitudes of the methane increases. However, the analysis shows the importance of also considering changes in the methane lower boundary condition and emissions. Especially when considering our results of the SSP3-7.0, this effect should be kept in mind because SSP3-7.0 shows even larger methane levels compared to SSP2-4.5.

7.4 Source apportionment method

The tagging method which we applied for source attribution is a diagnostic method. The method itself is mathematically correct, but it has some simplifications which influence the results, as discussed in detail by Mertens et al. (2018) and Butler et al. (2018). In addition, different ozone source attribution methods exist (e.g. Lelieveld and Dentener, 2000; Emmons et al., 2010; Butler et al., 2018). Our approach at-

tributes NO_x and VOC emissions at the same time, while the approach of Butler et al. (2018) tags either NO_x or VOC. Especially for the shipping sector but most likely also for the aviation and the land transport sector, which all have rather high NO_x emissions and low VOC emissions, our approach leads to lower contributions compared to the NO_x tagging approach (see also Butler et al., 2020).

7.5 Discrepancy between geographical distributions of the aviation emissions

We used the original aviation emissions from CMIP6. Thor et al. (2023) reported a discrepancy in the geographical distribution of the aviation emissions in CMIP6. This discrepancy leads to overestimated emissions in the Arctic and Antarctic regions and underestimated emissions in the tropics. Correcting for this discrepancy in the 2015 emissions leads to ozone RF of around 8 % larger and a 6 % larger relative reduction in the methane lifetime of the aviation emissions compared to the values discussed in the present paper (see Thor et al., 2023, for detailed analyses).

7.6 Future approaches

Future studies should aim to consider the effects of changed methane emissions and lower boundary conditions and the effects caused by climate and land-use change on the ozone and OH contributions of transport emissions and the associated radiative forcing and reductions in the methane lifetime. Due to the effects discussed above, such studies need a much more complicated design of the numerical experiments. Moreover, much longer integration times need to be taken into account to yield signals of the transport emissions larger than the internal variability (see for example Koffi et al., 2010). As the atmospheric chemistry response, and more importantly that of natural emissions, of climate change varies (e.g. Turnock et al., 2020), a multi-model approach would be of interest here; however only a few models feature ozone tagging approaches as used in the present study.

8 Conclusions and outlook

This paper presents an analysis of the effects of transport emissions from the sectors of land transport, aviation, and shipping on ozone and methane lifetime because the transport sector is an important source for ozone precursors. The aim is to support efforts to reduce transport emissions with a better understanding of the highly non-linear response of atmospheric chemistry on these emission changes. We investigated present-day conditions for 2015 and three projections of the emissions for 2050 according to the Shared Socioeconomic Pathways (SSPs) SSP1-1.9, SSP2-4.5, and SSP3-7.0. To do so, we performed a set of 5-year-long simulations with the chemistry-climate model EMAC. Atmospheric dynamics are kept identical in order to quantify the small signals of specific transport sectors. For the source attribution of the emission effects on ozone, OH, HO_2, and ozone-related precursors, we used a tagging method. Based on the contributions of the transport emissions to ozone and OH, we are able to calculate the radiative forcing of ozone attributable to these emissions. We also introduce a novel calculation of the relative reduction in the methane lifetime for all transport sectors based on the OH contributions, whereas previous studies used the so-called perturbation approach.

Our analyses of the model results can be summarized in the following most important findings.

- *Changes in transport emissions in SSPs*. In the SSP1 projection transport emissions are reduced strongly worldwide due to the high share of public transport, technological advancement including the adoption of newer technologies, increased use of high-speed trains, and overall reduced demand for transport. In the SSP2 projection the emissions of the land transport sector decrease compared to 2015 in most regions except South Asia. Here, the large increase in demand for mobility caused by an increasing population and insufficient pollution control and limited technological advancement lead to an increase in land transport emissions. Also, global NO_x emissions from aviation are doubled compared to 2015 due to increasing demands, while the shipping emissions are reduced slightly. In the SSP3 projection only Europe and North America show a larger decrease in land transport emissions in 2050 compared to 2015, while emissions increase in most other regions. The aviation emissions are similar to those in the SSP2 projection, and shipping emissions are reduced compared to SSP2 and to 2015, most likely due to international trade barriers in the narrative of the scenario.

- *Efficiency of ozone formation*. Due to the non-linearity of atmospheric chemistry, the response of atmospheric composition to the changed emissions is rather complex. In accordance with previous publications, we find a large efficiency of the ozone formation from aviation emissions, while ozone from land transport emissions in Europe and North America is formed rather inefficiently. A similar behaviour is also observed for OH, which is strongly bound to the NO_x–O_3 chemistry.

- *Atmospheric effects of SSP1 emissions*. Due to the strong decrease in emissions in SSP1, the non-linearity of the NO_x–O_3 chemistry compensates for some of the emission reductions. However, the total decrease in the emissions is so large that the contributions of the transport emissions to ozone and the associated radiative forcing decrease strongly. The non-linearity of the OH response and the associated relative reduction in the methane lifetimes is stronger than for the O_3 response. Accordingly, the (cooling) effect of the transport emissions on the climate by the decrease in the methane lifetime can become more important compared to the warming effect of O_3 because the reduction in the methane lifetime is larger than the increase in ozone.

- *Atmospheric effects of SSP2 emissions*. In the SSP2 projection the land transport emissions are reduced strongly in many regions, leading to a large reduction in the ozone contributions and associated radiative forcing. However, ozone formed from land transport emissions over South Asia have rather large radiative forcing, as this ozone is transported into the upper troposphere very efficiently. Therefore, the radiative forcing from global land transport emissions is reduced by only 15 %. Although the total NO_x emissions of the aviation sector are low compared to the land transport sector, the doubling of the aviation NO_x emissions in SSP2 compared to 2015 almost compensates for the reductions in the land transport and the shipping sector in terms of ozone RF. Accordingly, the total radiative forcing of the transport sector is similar in 2050 for SSP2 compared to 2015. The contributions to the methane lifetime show a similar behaviour.

- *Atmospheric effects of SSP3 emissions*. In the SSP3 projection land transport emissions in Europe and North America are reduced, but the non-linearity of the ozone chemistry strongly compensates for this reduction and the ozone contributions are not similarly reduced. In addition, due to a lack of international cooperation and increasing emissions in other parts of the world, the contribution of ozone from land transport transported via long-range transport increases over Europe and North America with SSP3 in 2050 compared to 2015. The global increase in land transport emissions, especially in South Asia, leads to an increase in the ozone radiative forcing from land transport emissions. Moreover, the doubling of aviation emissions compared to 2015 also leads to overall larger ozone radiative forcing and larger contributions to the methane lifetime of the transport sector in 2050 compared to 2015. Especially for the

results of SSP3 it should be kept in mind that we apply present-day methane levels in all simulations. Applying the methane levels for SSP3 in 2050 likely leads to even larger ozone increases, but the responses of the different emission sectors on the methane increase are very complex and require further investigations in follow-up studies.

– *Contributions of the transport sectors on O_3 and OH.* Overall, the land transport sector is the transport sector with the highest emissions and the largest effects on ozone and OH. In 2015, this is followed by shipping and aviation. Due to the increase in aviation emissions in SSP2 and SSP3 compared to 2015, caused by increased demand, and the reduction in shipping emissions in SSP2 and SSP3 compared to 2015, the effects of the aviation sector on ozone radiative forcing and methane lifetime are larger compared to the shipping sector.

– *Contributions from South Asia.* Already for the present day, land transport emissions from South Asia strongly contribute to tropospheric ozone. This contribution is projected to increase in SSP2 and SSP3. Given the large radiative efficiency of ozone formed from these emissions and their negative effects on air quality, very urgent mitigation policies aiming at a reduction in land transport emissions in this region are needed.

– *Implications for mitigation options.* The complex, nonlinear atmospheric responses of O_3 and OH highlight the necessity to investigate effects of possible mitigation options for the transport sector using state-of-the-art atmospheric chemistry models. These effects are overlooked if only emission reductions are analysed.

– *Tagging vs. perturbation approach.* The application of the source attribution method for OH and the diagnosed reductions in the methane lifetime yield results which deviate strongly from the results of the perturbation approach. With the 5 % perturbation the shipping sector leads to a larger reduction in the methane lifetime than the land transport and aviation sector. With the source attribution method emissions from the land transport sector lead to the largest reduction in the methane lifetime (around 7 times larger compared to a 5 % perturbation), followed by the shipping and the aviation sector. Such larger reductions in the methane lifetime also influence the total radiative forcing caused by the NO_x emissions which will be analysed in a follow-up study.

Due to the very complex response of atmospheric chemistry to emission changes, we did not consider the effects of climate change in our simulations. Also the effects of increased methane emissions were only investigated in a short sensitivity simulation. Future studies should incorporate both effects. In particular, for example, changes in lightning NO_x

emissions and biogenic emissions could also strongly influence contributions of land transport emissions to the atmospheric composition. A reduction in the ozone lifetime due to increased water vapour could reduce long-range transport or contributions from shipping. Moreover, in very strong mitigation cases, such as SSP1, the role of these natural emissions will be more and more important due to the nonlinearity of the ozone chemistry, as the effects of the transport emissions strongly depend on the background conditions. Such a study, however, would need much longer model integration times, and due to different responses of atmospheric composition by climate change by different models, a multimodel approach would be very valuable here. The lack of publicly available information on the detailed assumptions and trends in the transport sectors from the SSP narratives complicated the detailed interpretation of some of the results. For future studies it would therefore be very valuable if such important information on the developments in the transport sector would also be publicly available (e.g. for CMIP7).
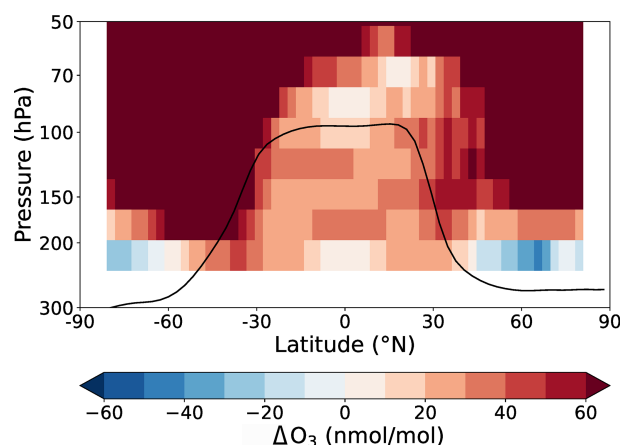
Appendix A

Figure A1. Absolute difference (in $nmol\,mol^{-1}$) between ozone mixing ratios from the PD simulation and the SWOOSH data. The SWOOSH data are interpolated horizontally onto the coarser EMAC grid. The EMAC data are interpolated vertically onto the coarser SWOOSH grid. All data are averages for 2013–2017. The colour scale is optimized for tropospheric ozone values and not for stratospheric values.

per is based on EMAC version 2.55. The exact set-up used to produce the results of this paper is archived at the German Climate Computing Center (DKRZ) and can be made available to members of the MESSy community upon request. The model results analysed in this study are available on request.

Author contributions. MM performed the model simulations and analysed the model results. SB assisted with the emission processing and performed the methane lifetime analyses. VG and VR developed the improved HO_x TAGGING needed for this study. JH designed and coordinated the experimental set-up. PJ supported the necessary model development and methane lifetime analyses. PG supported the model set-up and emission processing. AL performed analyses of the ozone non-linearity and emissions. SM, VG, and RNT helped to analyse the aircraft emissions. MR participated in the discussion regarding the experimental set-up and the analysis of the traffic projections in the SSPs. All authors supported the interpretation of the modelling results and contributed to the writing of the manuscript.

Disclaimer. Publisher's note: Copernicus Publications remains neutral with regard to jurisdictional claims made in the text, published maps, institutional affiliations, or any other geographical representation in this paper. While Copernicus Publications makes every effort to include appropriate place names, the final responsibility lies with the authors.

Special issue statement. This article is part of the special issue "Tropospheric Ozone Assessment Report Phase II (TOAR-II) Community Special Issue (ACP/AMT/BG/GMD inter-journal SI)". It is not associated with a conference.

References

Archibald, A. T., Neu, J. L., Elshorbany, Y. F., Cooper, O. R., Young, P. J., Akiyoshi, H., Cox, R. A., Coyle, M., Derwent, R. G., Deushi, M., Finco, A., Frost, G. J., Galbally, I. E., Gerosa, G., Granier, C., Griffiths, P. T., Hossaini, R., Hu, L., Jöckel, P., Josse, B., Lin, M. Y., Mertens, M., Morgenstern, O., Naja, M., Naik, V., Oltmans, S., Plummer, D. A., Revell, L. E., Saiz-Lopez, A., Saxena, P., Shin, Y. M., Shahid, I., Shallcross, D., Tilmes, S., Trickl, T., Wallington, T. J., Wang, T., Worden, H. M., and Zeng, G.: Tropospheric Ozone Assessment Report: A critical review of changes in the tropospheric ozone burden and budget from 1850 to 2100, Elementa: Sci. Anthropo., 8, 034, https://doi.org/10.1525/elementa.2020.034, 2020.

Bauer, N., Calvin, K., Emmerling, J., Fricko, O., Fujimori, S., Hilaire, J., Eom, J., Krey, V., Kriegler, E., Mouratiadou, I., Sytze de Boer, H., van den Berg, M., Carrara, S., Daioglou, V., Drouet, L., Edmonds, J. E., Gernaat, D., Havlik, P., Johnson, N., Klein, D., Kyle, P., Marangoni, G., Masui, T., Pietzcker, R. C., Strubegger, M., Wise, M., Riahi, K., and van Vuuren, D. P.: Shared Socio-Economic Pathways of the Energy Sector – Quantifying the Narratives, Global Environ. Change, 42, 316–330, https://doi.org/10.1016/j.gloenvcha.2016.07.006, 2017.

Bellouin, N., Quaas, J., Gryspeerdt, E., Kinne, S., Stier, P., Watson-Parris, D., Boucher, O., Carslaw, K. S., Christensen, M., Daniau, A.-L., Dufresne, J.-L., Feingold, G., Fiedler, S., Forster, P., Gettelman, A., Haywood, J. M., Lohmann, U., Malavelle, F., Mauritsen, T., McCoy, D. T., Myhre, G., Mülmenstädt, J., Neubauer, D., Possner, A., Rugenstein, M., Sato, Y., Schulz, M., Schwartz, S. E., Sourdeval, O., Storelvmo, T., Toll, V., Winker, D., and Stevens, B.: Bounding Global Aerosol Radiative Forcing of Climate Change, Rev. Geophys., 58, e2019RG000660, https://doi.org/10.1029/2019RG000660, 2020.

Butler, T., Lupascu, A., Coates, J., and Zhu, S.: TOAST 1.0: Tropospheric Ozone Attribution of Sources with Tagging for CESM 1.2.2, Geosci. Model Dev., 11, 2825–2840, https://doi.org/10.5194/gmd-11-2825-2018, 2018.

Butler, T., Lupascu, A., and Nalam, A.: Attribution of ground-level ozone to anthropogenic and natural sources of nitrogen oxides and reactive carbon in a global chemical transport model, Atmos. Chem. Phys., 20, 10707–10731, https://doi.org/10.5194/acp-20-10707-2020, 2020.

Clappier, A., Belis, C. A., Pernigotti, D., and Thunis, P.: Source apportionment and sensitivity analysis: two methodologies with two different purposes, Geosci. Model Dev., 10, 4245–4256, https://doi.org/10.5194/gmd-10-4245-2017, 2017.

Cohen, Y., Hauglustaine, D., Bellouin, N., Eastham, S., Lund, M. T., Matthes, S., Skowron, A., and Thor, R.: Impact of aircraft NOx and aerosol emissions on atmospheric composition : a model intercomparison, EGU General Assembly 2023, Vienna, Austria, 23–28 April 2023, EGU23-8605, https://doi.org/10.5194/egusphere-egu23-8605, 2023.

Cohen, Y., Hauglustaine, D., Bellouin, N., Lund, M. T., Matthes, S., Skowron, A., Thor, R., Bundke, U., Petzold, A., Rohs, S., Thouret, V., Zahn, A., and Ziereis, H.: Multi-model assessment of climatologies in the upper troposphere–lower stratosphere using the IAGOS data, EGUsphere [preprint], https://doi.org/10.5194/egusphere-2024-2208, 2024.

Dahlmann, K., Grewe, V., Ponater, M., and Matthes, S.: Quantifying the contributions of individual NO_x sources to the trend in ozone radiative forcing, Atmos. Environ., 45, 2860–2868, https://doi.org/10.1016/j.atmosenv.2011.02.071, 2011.

Davis, S. M., Rosenlof, K. H., Hassler, B., Hurst, D. F., Read, W. G., Vömel, H., Selkirk, H., Fujiwara, M., and Damadeo, R.: The Stratospheric Water and Ozone Satellite Homogenized (SWOOSH) database: a long-term database for climate studies, Earth Syst. Sci. Data, 8, 461–490, https://doi.org/10.5194/essd-8-461-2016, 2016.

Deckert, R., Jöckel, P., Grewe, V., Gottschaldt, K.-D., and Hoor, P.: A quasi chemistry-transport model mode for EMAC, Geosci. Model Dev., 4, 195–206, https://doi.org/10.5194/gmd-4-195-2011, 2011.

Dee, D. P., Uppala, S. M., Simmons, A. J., Berrisford, P., Poli, P., Kobayashi, S., Andrae, U., Balmaseda, M. A., Balsamo, G., Bauer, P., Bechtold, P., Beljaars, A. C. M., van de Berg, L., Bidlot, J., Bormann, N., Delsol, C., Dragani, R., Fuentes, M., Geer, A. J., Haimberger, L., Healy, S. B., Hersbach, H., Hólm, E. V., Isaksen, L., Kållberg, P., Köhler, M., Matricardi, M., McNally, A. P., Monge-Sanz, B. M., Morcrette, J.-J., Park, B.-K., Peubey, C., de Rosnay, P., Tavolato, C., Thépaut, J.-N., and Vitart, F.: The ERA-Interim reanalysis: configuration and performance of the data assimilation system, Q. J. Roy. Meteor. Soc., 137, 553–597, https://doi.org/10.1002/qj.828, 2011.

Derwent, R. G., Collins, W. J., Johnson, C. E., and Stevenson, D. S.: Transient Behaviour of Tropospheric Ozone Precursors in a Global 3-D CTM and Their Indirect Greenhouse Effects, 49, 463–487, https://doi.org/10.1023/A:1010648913655, 2001.

Dietmüller, S., Jöckel, P., Tost, H., Kunze, M., Gellhorn, C., Brinkop, S., Frömming, C., Ponater, M., Steil, B., Lauer, A., and Hendricks, J.: A new radiation infrastructure for the Modular Earth Submodel System (MESSy, based on version 2.51), Geosci. Model Dev., 9, 2209–2222, https://doi.org/10.5194/gmd-9-2209-2016, 2016.

Emmons, L. K., Walters, S., Hess, P. G., Lamarque, J.-F., Pfister, G. G., Fillmore, D., Granier, C., Guenther, A., Kinnison, D., Laepple, T., Orlando, J., Tie, X., Tyndall, G., Wiedinmyer, C., Baughcum, S. L., and Kloster, S.: Description and evaluation of the Model for Ozone and Related chemical Tracers, version 4 (MOZART-4), Geosci. Model Dev., 3, 43–67, https://doi.org/10.5194/gmd-3-43-2010, 2010.

Eyring, V., Stevenson, D. S., Lauer, A., Dentener, F. J., Butler, T., Collins, W. J., Ellingsen, K., Gauss, M., Hauglustaine, D. A., Isaksen, I. S. A., Lawrence, M. G., Richter, A., Rodriguez, J. M., Sanderson, M., Strahan, S. E., Sudo, K., Szopa, S., van Noije, T. P. C., and Wild, O.: Multi-model simulations of the impact of international shipping on Atmospheric Chemistry and Climate in 2000 and 2030, Atmos. Chem. Phys., 7, 757–780, https://doi.org/10.5194/acp-7-757-2007, 2007.

Feng, L., Smith, S. J., Braun, C., Crippa, M., Gidden, M. J., Hoesly, R., Klimont, Z., van Marle, M., van den Berg, M., and van der Werf, G. R.: The generation of gridded emissions data for CMIP6, Geosci. Model Dev., 13, 461–482, https://doi.org/10.5194/gmd-13-461-2020, 2020.

Fleming, Z. L., Doherty, R. M., von Schneidemesser, E., Malley, C. S., Cooper, O. R., Pinto, J. P., Colette, A., Xu, X., Simpson, D., Schultz, M. G., Lefohn, A. S., Hamad, S., Moolla, R., Solberg, S., and Feng, Z.: Tropospheric Ozone Assessment Report: Present-day ozone distribution and trends relevant to human health, Elementa: Sci. Anthropo., 6, 12, https://doi.org/10.1525/elementa.273, 2018.

Forster, P., Storelvmo, T., Armour, K., Collins, W., Dufresne, J.-L., Frame, D., Lunt, D., Mauritsen, T., Palmer, M., Watanabe, M., Wild, M., and Zhang, H.: The Earth's Energy Budget, Climate Feedbacks, and Climate Sensitivity, in: Climate Change 2021: The Physical Science Basis. Contribution of Working Group I to the Sixth Assessment Report of the Intergovernmental Panel on Climate Change, edited by: Masson-Delmotte, V., Zhai, P., Pirani, A., Connors, S. L., Péan, C., Berger, S., Caud, N., Chen, Y., Goldfarb, L., Gomis, M. I., Huang, M., Leitzell, K., Lonnoy, E., Matthews, J. B. R., Maycock, T. K., Waterfield, T., Yelekçi, O., Yu, R., and Zhou, B., book section 7, Cambridge University Press, Cambridge, UK and New York, NY, USA, https://doi.org/10.1017/9781009157896.009, 2021.

Fricko, O., Havlik, P., Rogelj, J., Klimont, Z., Gusti, M., Johnson, N., Kolp, P., Strubegger, M., Valin, H., Amann, M., Ermolieva, T., Forsell, N., Herrero, M., Heyes, C., Kindermann, G., Krey, V., McCollum, D. L., Obersteiner, M., Pachauri, S., Rao, S., Schmid, E., Schoepp, W., and Riahi, K.: The marker quantification of the Shared Socioeconomic Pathway 2: A middle-of-the-road scenario for the 21st century, Global Environ. Change, 42, 251–267, https://doi.org/10.1016/j.gloenvcha.2016.06.004, 2017.

Fujimori, S., Hasegawa, T., Masui, T., Takahashi, K., Herran, D. S., Dai, H., Hijioka, Y., and Kainuma, M.: SSP3: AIM implementation of Shared Socioeconomic Pathways, Global Environ. Change, 42, 268–283, https://doi.org/10.1016/j.gloenvcha.2016.06.009, 2017.

Gidden, M. J., Riahi, K., Smith, S. J., Fujimori, S., Luderer, G., Kriegler, E., van Vuuren, D. P., van den Berg, M., Feng, L., Klein, D., Calvin, K., Doelman, J. C., Frank, S., Fricko, O., Harmsen, M., Hasegawa, T., Havlik, P., Hilaire, J., Hoesly, R., Horing, J., Popp, A., Stehfest, E., and Takahashi, K.: Global emissions pathways under different socioeconomic scenarios for use in CMIP6: a dataset of harmonized emissions trajectories through the end of the century, Geosci. Model Dev., 12, 1443–1475, https://doi.org/10.5194/gmd-12-1443-2019, 2019.

Grange, S. K., Lee, J. D., Drysdale, W. S., Lewis, A. C., Hueglin, C., Emmenegger, L., and Carslaw, D. C.: COVID-19 lockdowns highlight a risk of increasing ozone pollution in Eu-

ropean urban areas, Atmos. Chem. Phys., 21, 4169–4185, https://doi.org/10.5194/acp-21-4169-2021, 2021.

Grewe, V. and Dameris, M.: Calculating the global mass exchange between stratosphere and troposphere, Ann. Geophys., 14, 431–442, https://doi.org/10.1007/s00585-996-0431-x, 1996.

Grewe, V., Brunner, D., Dameris, M., Grenfell, J., Hein, R., Shindell, D., and Staehelin, J.: Origin and variability of upper tropospheric nitrogen oxides and ozone at northern mid-latitudes, Atmos. Environ., 35, 3421–3433, https://doi.org/10.1016/S1352-2310(01)00134-0, 2001.

Grewe, V., Tsati, E., and Hoor, P.: On the attribution of contributions of atmospheric trace gases to emissions in atmospheric model applications, Geosci. Model Dev., 3, 487–499, https://doi.org/10.5194/gmd-3-487-2010, 2010.

Grewe, V., Tsati, E., Mertens, M., Frömming, C., and Jöckel, P.: Contribution of emissions to concentrations: the TAGGING 1.0 submodel based on the Modular Earth Submodel System (MESSy 2.52), Geosci. Model Dev., 10, 2615–2633, https://doi.org/10.5194/gmd-10-2615-2017, 2017.

Guenther, A., Hewitt, C. N., Erickson, D., Fall, R., Geron, C., Graedel, T., Harley, P., Klinger, L., Lerdau, M., Mckay, W. A., Pierce, T., Scholes, B., Steinbrecher, R., Tallamraju, R., Taylor, J., and Zimmerman, P.: A global model of natural volatile organic compound emissions, J. Geophys. Res., 100, 8873–8892, 1995.

Hauglustaine, D. A., Granier, C., Brasseur, G. P., and Mégie, G.: Impact of present aircraft emissions of nitrogen oxides on tropospheric ozone and climate forcing, Geophys. Res. Lett., 21, 2031–2034, https://doi.org/10.1029/94GL01729, 1994.

Hodnebrog, Ø., Berntsen, T. K., Dessens, O., Gauss, M., Grewe, V., Isaksen, I. S. A., Koffi, B., Myhre, G., Olivié, D., Prather, M. J., Stordal, F., Szopa, S., Tang, Q., van Velthoven, P., and Williams, J. E.: Future impact of traffic emissions on atmospheric ozone and OH based on two scenarios, Atmos. Chem. Phys., 12, 12211–12225, https://doi.org/10.5194/acp-12-12211-2012, 2012.

Hoesly, R. M., Smith, S. J., Feng, L., Klimont, Z., Janssens-Maenhout, G., Pitkanen, T., Seibert, J. J., Vu, L., Andres, R. J., Bolt, R. M., Bond, T. C., Dawidowski, L., Kholod, N., Kurokawa, J.-I., Li, M., Liu, L., Lu, Z., Moura, M. C. P., O'Rourke, P. R., and Zhang, Q.: Historical (1750–2014) anthropogenic emissions of reactive gases and aerosols from the Community Emissions Data System (CEDS), Geosci. Model Dev., 11, 369–408, https://doi.org/10.5194/gmd-11-369-2018, 2018.

Hoor, P., Borken-Kleefeld, J., Caro, D., Dessens, O., Endresen, O., Gauss, M., Grewe, V., Hauglustaine, D., Isaksen, I. S. A., Jöckel, P., Lelieveld, J., Myhre, G., Meijer, E., Olivie, D., Prather, M., Schnadt Poberaj, C., Shine, K. P., Staehelin, J., Tang, Q., van Aardenne, J., van Velthoven, P., and Sausen, R.: The impact of traffic emissions on atmospheric ozone and OH: results from QUANTIFY, Atmos. Chem. Phys., 9, 3113–3136, https://doi.org/10.5194/acp-9-3113-2009, 2009.

Janssens-Maenhout, G., Crippa, M., Guizzardi, D., Muntean, M., Schaaf, E., Dentener, F., Bergamaschi, P., Pagliari, V., Olivier, J. G. J., Peters, J. A. H. W., van Aardenne, J. A., Monni, S., Doering, U., Petrescu, A. M. R., Solazzo, E., and Oreggioni, G. D.: EDGAR v4.3.2 Global Atlas of the three major greenhouse gas emissions for the period 1970–2012, Earth Syst. Sci. Data, 11, 959–1002, https://doi.org/10.5194/essd-11-959-2019, 2019.

Jöckel, P., Tost, H., Pozzer, A., Brühl, C., Buchholz, J., Ganzeveld, L., Hoor, P., Kerkweg, A., Lawrence, M. G., Sander, R., Steil, B., Stiller, G., Tanarhte, M., Taraborrelli, D., van Aardenne, J., and Lelieveld, J.: The atmospheric chemistry general circulation model ECHAM5/MESSy1: consistent simulation of ozone from the surface to the mesosphere, Atmos. Chem. Phys., 6, 5067–5104, https://doi.org/10.5194/acp-6-5067-2006, 2006.

Jöckel, P., Kerkweg, A., Pozzer, A., Sander, R., Tost, H., Riede, H., Baumgaertner, A., Gromov, S., and Kern, B.: Development cycle 2 of the Modular Earth Submodel System (MESSy2), Geosci. Model Dev., 3, 717–752, https://doi.org/10.5194/gmd-3-717-2010, 2010.

Jöckel, P., Tost, H., Pozzer, A., Kunze, M., Kirner, O., Brenninkmeijer, C. A. M., Brinkop, S., Cai, D. S., Dyroff, C., Eckstein, J., Frank, F., Garny, H., Gottschaldt, K.-D., Graf, P., Grewe, V., Kerkweg, A., Kern, B., Matthes, S., Mertens, M., Meul, S., Neumaier, M., Nützel, M., Oberländer-Hayn, S., Ruhnke, R., Runde, T., Sander, R., Scharffe, D., and Zahn, A.: Earth System Chemistry integrated Modelling (ESCiMo) with the Modular Earth Submodel System (MESSy) version 2.51, Geosci. Model Dev., 9, 1153–1200, https://doi.org/10.5194/gmd-9-1153-2016, 2016.

KC, S. and Lutz, W.: The human core of the shared socioeconomic pathways: Population scenarios by age, sex and level of education for all countries to 2100, Global Environ. Change, 42, 181–192, https://doi.org/10.1016/j.gloenvcha.2014.06.004, 2017.

Kerkweg, A., Sander, R., Tost, H., and Jöckel, P.: Technical note: Implementation of prescribed (OFFLEM), calculated (ONLEM), and pseudo-emissions (TNUDGE) of chemical species in the Modular Earth Submodel System (MESSy), Atmos. Chem. Phys., 6, 3603–3609, https://doi.org/10.5194/acp-6-3603-2006, 2006.

Koffi, B., Szopa, S., Cozic, A., Hauglustaine, D., and van Velthoven, P.: Present and future impact of aircraft, road traffic and shipping emissions on global tropospheric ozone, Atmos. Chem. Phys., 10, 11681–11705, https://doi.org/10.5194/acp-10-11681-2010, 2010.

Lee, D., Fahey, D., Skowron, A., Allen, M., Burkhardt, U., Chen, Q., Doherty, S., Freeman, S., Forster, P., Fuglestvedt, J., Gettelman, A., León, R. D., Lim, L., Lund, M., Millar, R., Owen, B., Penner, J., Pitari, G., Prather, M., Sausen, R., and Wilcox, L.: The contribution of global aviation to anthropogenic climate forcing for 2000 to 2018, Atmos. Environ., 244, 117834, https://doi.org/10.1016/j.atmosenv.2020.117834, 2021.

Lelieveld, J. and Dentener, F. J.: What controls tropospheric ozone?, J. Geophys. Res.-Atmos., 105, 3531–3551, https://doi.org/10.1029/1999JD901011, 2000.

Lin, M., Horowitz, L. W., Xie, Y., Paulot, F., Malyshev, S., Shevliakova, E., Finco, A., Gerosa, G., Kubistin, D., and Pilegaard, K.: Vegetation feedbacks during drought exacerbate ozone air pollution extremes in Europe, Nat. Clim. Change, 10, 444–451, https://doi.org/10.1038/s41558-020-0743-y, 2020.

Maruhashi, J., Mertens, M., Grewe, V., and Dedoussi, I. C.: A multi-method assessment of the regional sensitivities between flight altitude and short-term O_3 climate warming from aircraft NO_x emissions, Environ. Res. Lett., 19, 054007, https://doi.org/10.1088/1748-9326/ad376a, 2024.

Matthes, S., Lim, L., Burkhardt, U., Dahlmann, K., Dietmüller, S., Grewe, V., Haslerud, A. S., Hendricks, J., Owen, B., Pitari, G., Righi, M., and Skowron, A.: Mitigation of Non-CO_2 Aviation's

Climate Impact by Changing Cruise Altitudes, Aerospace, 8, 36, https://doi.org/10.3390/aerospace8020036, 2021.

Matthias, V., Aulinger, A., Backes, A., Bieser, J., Geyer, B., Quante, M., and Zeretzke, M.: The impact of shipping emissions on air pollution in the greater North Sea region – Part 2: Scenarios for 2030, Atmos. Chem. Phys., 16, 759–776, https://doi.org/10.5194/acp-16-759-2016, 2016.

Matthias, V., Quante, M., Arndt, J. A., Badeke, R., Fink, L., Petrik, R., Feldner, J., Schwarzkopf, D., Link, E.-M., Ramacher, M. O. P., and Wedemann, R.: The role of emission reductions and the meteorological situation for air quality improvements during the COVID-19 lockdown period in central Europe, Atmos. Chem. Phys., 21, 13931–13971, https://doi.org/10.5194/acp-21-13931-2021, 2021.

McDuffie, E. E., Smith, S. J., O'Rourke, P., Tibrewal, K., Venkataraman, C., Marais, E. A., Zheng, B., Crippa, M., Brauer, M., and Martin, R. V.: A global anthropogenic emission inventory of atmospheric pollutants from sector- and fuel-specific sources (1970–2017): an application of the Community Emissions Data System (CEDS), Earth Syst. Sci. Data, 12, 3413–3442, https://doi.org/10.5194/essd-12-3413-2020, 2020.

Mertens, M., Grewe, V., Rieger, V. S., and Jöckel, P.: Revisiting the contribution of land transport and shipping emissions to tropospheric ozone, Atmos. Chem. Phys., 18, 5567–5588, https://doi.org/10.5194/acp-18-5567-2018, 2018.

Mertens, M., Kerkweg, A., Grewe, V., Jöckel, P., and Sausen, R.: Are contributions of emissions to ozone a matter of scale? – a study using MECO(n) (MESSy v2.50), Geosci. Model Dev., 13, 363–383, https://doi.org/10.5194/gmd-13-363-2020, 2020a.

Mertens, M., Kerkweg, A., Grewe, V., Jöckel, P., and Sausen, R.: Attributing ozone and its precursors to land transport emissions in Europe and Germany, Atmos. Chem. Phys., 20, 7843–7873, https://doi.org/10.5194/acp-20-7843-2020, 2020b.

Mertens, M., Jöckel, P., Matthes, S., Nützel, M., Grewe, V., and Sausen, R.: COVID-19 induced lower-tropospheric ozone changes, Environ. Res. Lett., 16, 064005, https://doi.org/10.1088/1748-9326/abf191, 2021.

Mills, G., Pleijel, H., Malley, C. S., Sinha, B., Cooper, O. R., Schultz, M. G., Neufeld, H. S., Simpson, D., Sharps, K., Feng, Z., Gerosa, G., Harmens, H., Kobayashi, K., Saxena, P., Paoletti, E., Sinha, V., and Xu, X.: Tropospheric Ozone Assessment Report: Present-day tropospheric ozone distribution and trends relevant to vegetation, Elementa: Sci. Anthropo., 6, 47, https://doi.org/10.1525/elementa.302, 2018.

Monks, P. S., Archibald, A. T., Colette, A., Cooper, O., Coyle, M., Derwent, R., Fowler, D., Granier, C., Law, K. S., Mills, G. E., Stevenson, D. S., Tarasova, O., Thouret, V., von Schneidemesser, E., Sommariva, R., Wild, O., and Williams, M. L.: Tropospheric ozone and its precursors from the urban to the global scale from air quality to short-lived climate forcer, Atmos. Chem. Phys., 15, 8889–8973, https://doi.org/10.5194/acp-15-8889-2015, 2015.

Naik, V., Voulgarakis, A., Fiore, A. M., Horowitz, L. W., Lamarque, J.-F., Lin, M., Prather, M. J., Young, P. J., Bergmann, D., Cameron-Smith, P. J., Cionni, I., Collins, W. J., Dalsøren, S. B., Doherty, R., Eyring, V., Faluvegi, G., Folberth, G. A., Josse, B., Lee, Y. H., MacKenzie, I. A., Nagashima, T., van Noije, T. P. C., Plummer, D. A., Righi, M., Rumbold, S. T., Skeie, R., Shindell, D. T., Stevenson, D. S., Strode, S., Sudo, K., Szopa, S., and Zeng, G.: Preindustrial to present-day changes in tropospheric hydroxyl

radical and methane lifetime from the Atmospheric Chemistry and Climate Model Intercomparison Project (ACCMIP), Atmos. Chem. Phys., 13, 5277–5298, https://doi.org/10.5194/acp-13-5277-2013, 2013.

O'Neill, B. C., Kriegler, E., Ebi, K. L., Kemp-Benedict, E., Riahi, K., Rothman, D. S., van Ruijven, B. J., van Vuuren, D. P., Birkmann, J., Kok, K., Levy, M., and Solecki, W.: The roads ahead: Narratives for shared socioeconomic pathways describing world futures in the 21st century, Global Environ. Change, 42, 169–180, https://doi.org/10.1016/j.gloenvcha.2015.01.004, 2017.

Pletzer, J. and Grewe, V.: Sensitivities of atmospheric composition and climate to altitude and latitude of hypersonic aircraft emissions, Atmos. Chem. Phys., 24, 1743–1775, https://doi.org/10.5194/acp-24-1743-2024, 2024.

Pletzer, J., Hauglustaine, D., Cohen, Y., Jöckel, P., and Grewe, V.: The climate impact of hydrogen-powered hypersonic transport, Atmos. Chem. Phys., 22, 14323–14354, https://doi.org/10.5194/acp-22-14323-2022, 2022.

Popp, A., Calvin, K., Fujimori, S., Havlik, P., Humpenöder, F., Stehfest, E., Bodirsky, B. L., Dietrich, J. P., Doelmann, J. C., Gusti, M., Hasegawa, T., Kyle, P., Obersteiner, M., Tabeau, A., Takahashi, K., Valin, H., Waldhoff, S., Weindl, I., Wise, M., Kriegler, E., Lotze-Campen, H., Fricko, O., Riahi, K., and van Vuuren, D. P.: Land-use futures in the shared socio-economic pathways, Global Environ.l Change, 42, 331–345, https://doi.org/10.1016/j.gloenvcha.2016.10.002, 2017.

Putero, D., Cristofanelli, P., Chang, K.-L., Dufour, G., Beachley, G., Couret, C., Effertz, P., Jaffe, D. A., Kubistin, D., Lynch, J., Petropavlovskikh, I., Puchalski, M., Sharac, T., Sive, B. C., Steinbacher, M., Torres, C., and Cooper, O. R.: Fingerprints of the COVID-19 economic downturn and recovery on ozone anomalies at high-elevation sites in North America and Western Europe, EGUsphere [preprint], https://doi.org/10.5194/egusphere-2023-1737, 2023.

Rao, S., Klimont, Z., Smith, S. J., Van Dingenen, R., Dentener, F., Bouwman, L., Riahi, K., Amann, M., Bodirsky, B. L., van Vuuren, D. P., Aleluia Reis, L., Calvin, K., Drouet, L., Fricko, O., Fujimori, S., Gernaat, D., Havlik, P., Harmsen, M., Hasegawa, T., Heyes, C., Hilaire, J., Luderer, G., Masui, T., Stehfest, E., Strefler, J., van der Sluis, S., and Tavoni, M.: Future air pollution in the Shared Socio-economic Pathways, Global Environ. Change, 42, 346–358, https://doi.org/10.1016/j.gloenvcha.2016.05.012, 2017.

Rap, A., Richards, N. A. D., Forster, P. M., Monks, S. A., Arnold, S. R., and Chipperfield, M. P.: Satellite constraint on the tropospheric ozone radiative effect, Geophys. Res. Lett., 42, 5074–5081, https://doi.org/10.1002/2015GL064037, 2015.

Riahi, K., van Vuuren, D. P., Kriegler, E., Edmonds, J., O'Neill, B. C., Fujimori, S., Bauer, N., Calvin, K., Dellink, R., Fricko, O., Lutz, W., Popp, A., Cuaresma, J. C., KC, S., Leimbach, M., Jiang, L., Kram, T., Rao, S., Emmerling, J., Ebi, K., Hasegawa, T., Havlik, P., Humpenöder, F., Da Silva, L. A., Smith, S., Stehfest, E., Bosetti, V., Eom, J., Gernaat, D., Masui, T., Rogelj, J., Strefler, J., Drouet, L., Krey, V., Luderer, G., Harmsen, M., Takahashi, K., Baumstark, L., Doelman, J. C., Kainuma, M., Klimont, Z., Marangoni, G., Lotze-Campen, H., Obersteiner, M., Tabeau, A., and Tavoni, M.: The Shared Socioeconomic Pathways and their energy, land use, and greenhouse gas emissions

implications: An overview, Global Environ. Change, 42, 153–168, https://doi.org/10.1016/j.gloenvcha.2016.05.009, 2017.

Rieger, V. S., Mertens, M., and Grewe, V.: An advanced method of contributing emissions to short-lived chemical species (OH and HO2): the TAGGING 1.1 submodel based on the Modular Earth Submodel System (MESSy 2.53), Geosci. Model Dev., 11, 2049–2066, https://doi.org/10.5194/gmd-11-2049-2018, 2018.

Riese, M., Ploeger, F., Rap, A., Vogel, B., Konopka, P., Dameris, M., and Forster, P.: Impact of uncertainties in atmospheric mixing on simulated UTLS composition and related radiative effects, J. Geophys. Res.-Atmos., 117, D16, https://doi.org/10.1029/2012JD017751, 2012.

Righi, M., Hendricks, J., and Sausen, R.: The global impact of the transport sectors on atmospheric aerosol in 2030 – Part 1: Land transport and shipping, Atmos. Chem. Phys., 15, 633–651, https://doi.org/10.5194/acp-15-633-2015, 2015.

Righi, M., Hendricks, J., and Brinkop, S.: The global impact of the transport sectors on the atmospheric aerosol and the resulting climate effects under the Shared Socioeconomic Pathways (SSPs), Earth Syst. Dynam., 14, 835–859, https://doi.org/10.5194/esd-14-835-2023, 2023.

Roeckner, E., Bäuml, G., Bonaventura, L., Brokopf, R., Esch, M., Giorgetta, M., Hagemann, S., Kirchner, I., Kornblueh, L., Manzini, E., Rhodin, A., Schlese, U., Schulzweida, U., and Tompkins, A.: The atmospheric general circulation model ECHAM5. PART I: Model description, MPI-Report 349, Max Planck Institut für Meteorologie in Hamburg, Deutschland, available at: https://pure.mpg.de/rest/items/item_995269_2/component/file_995268/content (last access: 12 August 2024), 2003.

Roeckner, E., Brokopf, R., Esch, M., Giorgetta, M., Hagemann, S., Kornblueh, L., Manzini, E., Schlese, U., and Schulzweida, U.: Sensitivity of Simulated Climate to Horizontal and Vertical Resolution in the ECHAM5 Atmosphere Model, J. Climate, 19, 3771–3791, https://doi.org/10.1175/jcli3824.1, 2006.

Sander, R., Baumgaertner, A., Gromov, S., Harder, H., Jöckel, P., Kerkweg, A., Kubistin, D., Regelin, E., Riede, H., Sandu, A., Taraborrelli, D., Tost, H., and Xie, Z.-Q.: The atmospheric chemistry box model CAABA/MECCA-3.0, Geosci. Model Dev., 4, 373–380, https://doi.org/10.5194/gmd-4-373-2011, 2011.

Sander, R., Jöckel, P., Kirner, O., Kunert, A. T., Landgraf, J., and Pozzer, A.: The photolysis module JVAL-14, compatible with the MESSy standard, and the JVal PreProcessor (JVPP), Geosci. Model Dev., 7, 2653–2662, https://doi.org/10.5194/gmd-7-2653-2014, 2014.

Schumann, U. and Huntrieser, H.: The global lightning-induced nitrogen oxides source, Atmos. Chem. Phys., 7, 3823–3907, https://doi.org/10.5194/acp-7-3823-2007, 2007.

Seinfeld, J. H. and Pandis, S. N.: Atmospheric Chemistry and Physics: From Air Pollution to Climate Change, Wiley, Seinfeld & Pandis, 2006.

Sillman, S.: The use of NO_y, H_2O_2, and HNO_3 as indicators for ozone-NO_x-hydrocarbon sensitivity in urban locations, J. Geophys. Res.-Atmos., 100, 14175–14188, https://doi.org/10.1029/94JD02953, 1995.

Stevenson, D. S., Young, P. J., Naik, V., Lamarque, J.-F., Shindell, D. T., Voulgarakis, A., Skeie, R. B., Dalsoren, S. B., Myhre, G., Berntsen, T. K., Folberth, G. A., Rumbold, S. T., Collins, W. J., MacKenzie, I. A., Doherty, R. M., Zeng, G., van Noije, T. P. C.,

Strunk, A., Bergmann, D., Cameron-Smith, P., Plummer, D. A., Strode, S. A., Horowitz, L., Lee, Y. H., Szopa, S., Sudo, K., Nagashima, T., Josse, B., Cionni, I., Righi, M., Eyring, V., Conley, A., Bowman, K. W., Wild, O., and Archibald, A.: Tropospheric ozone changes, radiative forcing and attribution to emissions in the Atmospheric Chemistry and Climate Model Intercomparison Project (ACCMIP), Atmos. Chem. Phys., 13, 3063–3085, https://doi.org/10.5194/acp-13-3063-2013, 2013.

Stohl, A., Aamaas, B., Amann, M., Baker, L. H., Bellouin, N., Berntsen, T. K., Boucher, O., Cherian, R., Collins, W., Daskalakis, N., Dusinska, M., Eckhardt, S., Fuglestvedt, J. S., Harju, M., Heyes, C., Hodnebrog, Ø., Hao, J., Im, U., Kanakidou, M., Klimont, Z., Kupiainen, K., Law, K. S., Lund, M. T., Maas, R., MacIntosh, C. R., Myhre, G., Myriokefalitakis, S., Olivié, D., Quaas, J., Quennehen, B., Raut, J.-C., Rumbold, S. T., Samset, B. H., Schulz, M., Seland, Ø., Shine, K. P., Skeie, R. B., Wang, S., Yttri, K. E., and Zhu, T.: Evaluating the climate and air quality impacts of short-lived pollutants, Atmos. Chem. Phys., 15, 10529–10566, https://doi.org/10.5194/acp-15-10529-2015, 2015.

Szopa, S., Naik, V., Adhikary, B., Artaxo, P., Berntsen, T., Collins, W. D., Fuzzi, S., Gallardo, L., Kiendler-Scharr, A., Klimont, Z., Liao, H., Unger, N., and Zanis, P.: Short-Lived Climate Forcers. In Climate Change 2021: The Physical Science Basis. Contribution of Working Group I to the Sixth Assessment Report of the Intergovernmental Panel on Climate Change, edited by: Masson-Delmotte, V., Zhai, P., Pirani, A., Connors, S. L., Péan, C., Berger, S., Caud, N., Chen, Y., Goldfarb, L., Gomis, M. I., Huang, M., Leitzell, K., Lonnoy, E., Matthews, J. B. R., Maycock, T. K., Waterfield, T., Yelekçi, O., Yu, R., and Zhou, B., Cambridge University Press, Cambridge, United Kingdom and New York, NY, USA, 817–922 pp., https://doi.org/10.1017/9781009157896.008, 2021.

Søvde, O. A., Matthes, S., Skowron, A., Iachetti, D., Lim, L., Owen, B., Øivind Hodnebrog, Di Genova, G., Pitari, G., Lee, D. S., Myhre, G., and Isaksen, I. S.: Aircraft emission mitigation by changing route altitude: A multi-model estimate of aircraft NO_x emission impact on O_3 photochemistry, Atmos. Environ., 95, 468–479, https://doi.org/10.1016/j.atmosenv.2014.06.049, 2014.

Taylor, K. E., Stouffer, R. J., and Meehl, G. A.: An Overview of CMIP5 and the Experiment Design, B. Am. Meteorol. Soc., 93, 485–498, https://doi.org/10.1175/BAMS-D-11-00094.1, 2012.

Terrenoire, E., Hauglustaine, D. A., Cohen, Y., Cozic, A., Valorso, R., Lefèvre, F., and Matthes, S.: Impact of present and future aircraft NO_x and aerosol emissions on atmospheric composition and associated direct radiative forcing of climate, Atmos. Chem. Phys., 22, 11987–12023, https://doi.org/10.5194/acp-22-11987-2022, 2022.

Thor, R. N., Mertens, M., Matthes, S., Righi, M., Hendricks, J., Brinkop, S., Graf, P., Grewe, V., Jöckel, P., and Smith, S.: An inconsistency in aviation emissions between CMIP5 and CMIP6 and the implications for short-lived species and their radiative forcing, Geosci. Model Dev., 16, 1459–1466, https://doi.org/10.5194/gmd-16-1459-2023, 2023.

Tost, H., Jöckel, P., Kerkweg, A., Sander, R., and Lelieveld, J.: Technical note: A new comprehensive SCAVenging submodel for global atmospheric chemistry modelling, Atmos. Chem. Phys., 6, 565–574, https://doi.org/10.5194/acp-6-565-2006, 2006.

Turnock, S. T., Allen, R. J., Andrews, M., Bauer, S. E., Deushi, M., Emmons, L., Good, P., Horowitz, L., John, J. G., Michou, M., Nabat, P., Naik, V., Neubauer, D., O'Connor, F. M., Olivié, D., Oshima, N., Schulz, M., Sellar, A., Shim, S., Takemura, T., Tilmes, S., Tsigaridis, K., Wu, T., and Zhang, J.: Historical and future changes in air pollutants from CMIP6 models, Atmos. Chem. Phys., 20, 14547–14579, https://doi.org/10.5194/acp-20-14547-2020, 2020.

van Vuuren, D. P., Stehfest, E., Gernaat, D. E., Doelman, J. C., van den Berg, M., Harmsen, M., de Boer, H. S., Bouwman, L. F., Daioglou, V., Edelenbosch, O. Y., Girod, B., Kram, T., Lassaletta, L., Lucas, P. L., van Meijl, H., Müller, C., van Ruijven, B. J., van der Sluis, S., and Tabeau, A.: Energy, land-use and greenhouse gas emissions trajectories under a green growth paradigm, Global Environ. Change, 42, 237–250, https://doi.org/10.1016/j.gloenvcha.2016.05.008, 2017.

von Kuhlmann, R., Lawrence, M. G., Pöschl, U., and Crutzen, P. J.: Sensitivities in global scale modeling of isoprene, Atmos. Chem. Phys., 4, 1–17, https://doi.org/10.5194/acp-4-1-2004, 2004.

von Schneidemesser, E., Monks, P. S., Allan, J. D., Bruhwiler, L., Forster, P., Fowler, D., Lauer, A., Morgan, W. T., Paasonen, P., Righi, M., Sindelarova, K., and Sutton, M. A.: Chemistry and the Linkages between Air Quality and Climate Change, Chem. Rev., 115, 3856–3897, https://doi.org/10.1021/acs.chemrev.5b00089, 2015.

Voulgarakis, A., Naik, V., Lamarque, J.-F., Shindell, D. T., Young, P. J., Prather, M. J., Wild, O., Field, R. D., Bergmann, D., Cameron-Smith, P., Cionni, I., Collins, W. J., Dalsøren, S. B., Doherty, R. M., Eyring, V., Faluvegi, G., Folberth, G. A., Horowitz, L. W., Josse, B., MacKenzie, I. A., Nagashima, T., Plummer, D. A., Righi, M., Rumbold, S. T., Stevenson, D. S., Strode, S. A., Sudo, K., Szopa, S., and Zeng, G.: Analysis of present day and future OH and methane lifetime in the ACCMIP simulations, Atmos. Chem. Phys., 13, 2563–2587, https://doi.org/10.5194/acp-13-2563-2013, 2013.

Wang, H., Lu, X., Jacob, D. J., Cooper, O. R., Chang, K.-L., Li, K., Gao, M., Liu, Y., Sheng, B., Wu, K., Wu, T., Zhang, J., Sauvage, B., Nédélec, P., Blot, R., and Fan, S.: Global tropospheric ozone trends, attributions, and radiative impacts in 1995–2017: an integrated analysis using aircraft (IAGOS) observations, ozonesonde, and multi-decadal chemical model simulations, Atmos. Chem. Phys., 22, 13753–13782, https://doi.org/10.5194/acp-22-13753-2022, 2022.

Wang, L., Tai, A. P. K., Tam, C.-Y., Sadiq, M., Wang, P., and Cheung, K. K. W.: Impacts of future land use and land cover change on mid-21st-century surface ozone air quality: distinguishing between the biogeophysical and biogeochemical effects, Atmos. Chem. Phys., 20, 11349–11369, https://doi.org/10.5194/acp-20-11349-2020, 2020.

Wang, Z. S., Chien, C.-J., and Tonnesen, G. S.: Development of a tagged species source apportionment algorithm to characterize three-dimensional transport and transformation of precursors and secondary pollutants, J. Geophys. Res.-Atmos., 114, d21206, https://doi.org/10.1029/2008JD010846, 2009.

Wesely, M. and Hicks, B.: A review of the current status of knowledge on dry deposition, Atmos. Environ., 34, 2261–2282, https://doi.org/10.1016/S1352-2310(99)00467-7, 2000.

Wild, O., Fiore, A. M., Shindell, D. T., Doherty, R. M., Collins, W. J., Dentener, F. J., Schultz, M. G., Gong, S., MacKenzie, I. A., Zeng, G., Hess, P., Duncan, B. N., Bergmann, D. J., Szopa, S., Jonson, J. E., Keating, T. J., and Zuber, A.: Modelling future changes in surface ozone: a parameterized approach, Atmos. Chem. Phys., 12, 2037–2054, https://doi.org/10.5194/acp-12-2037-2012, 2012.

Wu, S., Duncan, B. N., Jacob, D. J., Fiore, A. M., and Wild, O.: Chemical nonlinearities in relating intercontinental ozone pollution to anthropogenic emissions, Geophys. Res. Lett., 36, l05806, https://doi.org/10.1029/2008GL036607, 2009.

Wu, S., Mickley, L. J., Kaplan, J. O., and Jacob, D. J.: Impacts of changes in land use and land cover on atmospheric chemistry and air quality over the 21st century, Atmos. Chem. Phys., 12, 1597–1609, https://doi.org/10.5194/acp-12-1597-2012, 2012.

Yienger, J. J. and Levy, H.: Empirical model of global soil-biogenic NOx emissions, J. Geophys. Res.-Atmos., 100, 11447–11464, https://doi.org/10.1029/95JD00370, 1995.

Young, P. J., Archibald, A. T., Bowman, K. W., Lamarque, J.-F., Naik, V., Stevenson, D. S., Tilmes, S., Voulgarakis, A., Wild, O., Bergmann, D., Cameron-Smith, P., Cionni, I., Collins, W. J., Dalsøren, S. B., Doherty, R. M., Eyring, V., Faluvegi, G., Horowitz, L. W., Josse, B., Lee, Y. H., MacKenzie, I. A., Nagashima, T., Plummer, D. A., Righi, M., Rumbold, S. T., Skeie, R. B., Shindell, D. T., Strode, S. A., Sudo, K., Szopa, S., and Zeng, G.: Pre-industrial to end 21st century projections of tropospheric ozone from the Atmospheric Chemistry and Climate Model Intercomparison Project (ACCMIP), Atmos. Chem. Phys., 13, 2063–2090, https://doi.org/10.5194/acp-13-2063-2013, 2013.

Zanis, P., Akritidis, D., Turnock, S., Naik, V., Szopa, S., Georgoulias, A. K., Bauer, S. E., Deushi, M., Horowitz, L. W., Keeble, J., Sager, P. L., O'Connor, F. M., Oshima, N., Tsigaridis, K., and van Noije, T.: Climate change penalty and benefit on surface ozone: a global perspective based on CMIP6 earth system models, Environ. Res. Lett., 17, 024014, https://doi.org/10.1088/1748-9326/ac4a34, 2022.

Zhang, Y., Cooper, O. R., Gaudel, A., Thompson, A. M., Nédélec, P., Ogino, S.-Y., and West, J. J.: Tropospheric ozone change from 1980 to 2010 dominated by equatorward redistribution of emissions, Nat. Geosci., 9, 875–879, https://doi.org/10.1038/ngeo2827, 2016.